

國立交通大學
機械工程學系

利用 CESE 方法驗證一維波茲曼方程式

**One-Dimension Model Boltzmann Equation Solver Using
the CESE Method**

研究生：吳玟琪

指導教授：吳宗信 博士

中華民國九十七年 7 月

利用 CESE 方法驗證一維波滋曼方程式

**One-Dimension Model Boltzmann Equation Solver Using
the CESE Method**

研 究 生:吳玟琪

Student: Wun-Ci Wu

指 導 教 授:吳宗信 博士

Advisor: Dr. Jong-Shinn Wu

國立交通大學

機械工程學系

碩 士 論 文

A Thesis

Submitted to Institute of Mechanical Engineering

College of Engineering

National Chiao Tung University

in partial Fulfillment of the Requirements

for the Degree of

Master of Science

in

Mechanical Engineering

July 2008

Hsinchu, Taiwan

中華民國九十七年七月

利用 CESE 方法驗證一維波滋曼方程式

學生：吳玟琪

指導教授：吳宗信

國立交通大學機械工程學系

摘要

本文模擬重點是利用時空守恆元解元(CESE)對一維波滋曼方程式求解，CESE 方法的好處有：(1) 在數值不連續的地方有精確的數值解，(2) 邊界幾乎不會反彈，(3) 和蒙地卡羅(DSMC)方法相比，CESE 用在計算的成本相對要小很多，在本文裡，如何利用 CESE 對一維的尤拉方程式和波滋曼方程式的離散有詳細的介紹，我們模擬了五個 Riemann problems，Riemann problem 用來理解雙曲線偏微分方程式是最好用的，像歐拉方程，因為所有 Shock 和 Rarefaction waves 的現象都會出現。

模擬結果發現，CESE Method 不但可以減少大量的計算時間，在流體不連續的地方也可以的到很好的數值解，在這五個模擬的 case 裡，Rarefaction Wave 和 Shock 跟 Riemann problem 的 exact solution 很相似，但在 contact 的部份差異就比較大，最後，我們還利用 Test 1 的初始條件，模擬了不同的 Knudsen number，從 1 到 1E-20，結果顯示，當 Knudsen number 越小，結果也就越接近 Riemann problem 的 exact solution，未來，我們希望可以利用 CESE，並且結合 Model Boltzmann equation 和 Navier-Stork equation 來模擬 Shock wave 的問題。

One-Dimension Model Boltzmann Equation Solver Using the CESE Method

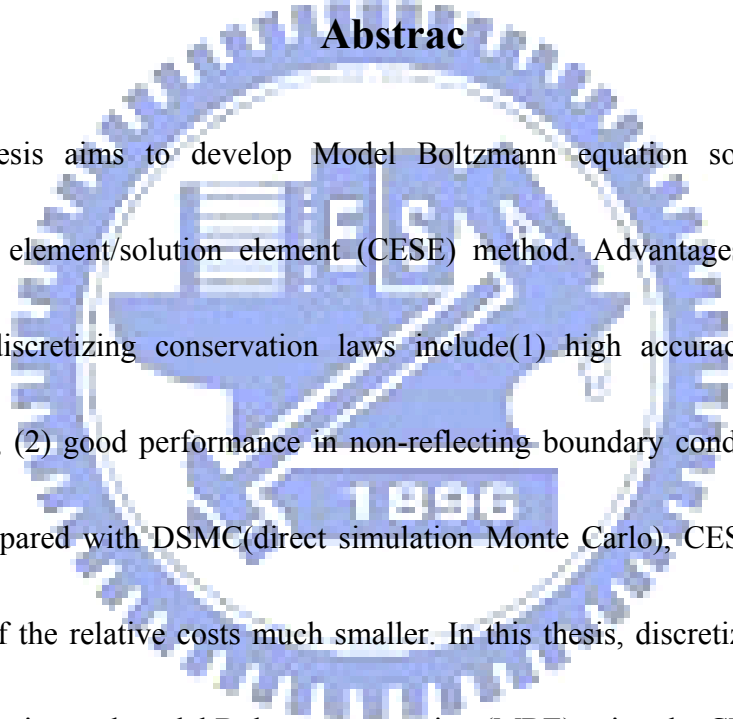
Student: W. C. Wu

Advisor: Dr. J. S. Wu

Department of Mechanical Engineering

National Chiao-Tung University

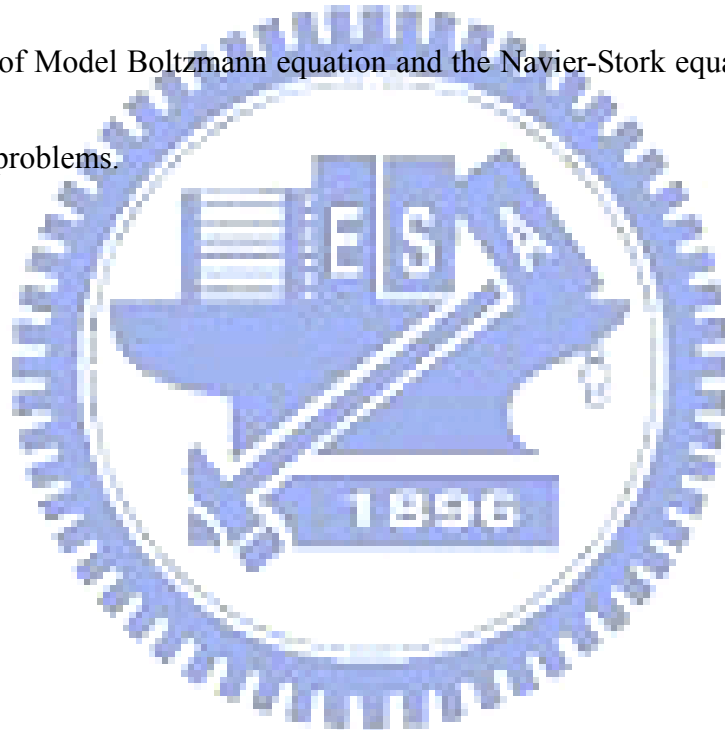
Abstrac

The logo of National Chiao-Tung University is a circular emblem with a gear-like outer border. Inside the circle, there is a stylized building and the year '1896' at the bottom. The word 'CESE' is written across the center of the emblem.

This thesis aims to develop Model Boltzmann equation solver using the conservation element/solution element (CESE) method. Advantages of the CESE method in discretizing conservation laws include (1) high accuracy in capturing discontinuity, (2) good performance in non-reflecting boundary condition treatment, and (3) Compared with DSMC (direct simulation Monte Carlo), CESE spent on the calculation of the relative costs much smaller. In this thesis, discretizations for both 1D Euler equation and model Boltzmann equation (MBE) using the CESE method are described in detail. We simulated five Riemann problems. The Riemann problem is very useful for the understanding of hyperbolic partial differential equation like the Euler equations because all properties like Shocks, Rarefaction waves appear as characteristics in the solution.

The results showed that, CESE Method can reduce a lot of calculus coast, in

discontinue can also be a very good simulation answer , in the five simulation cases, rarefaction and shock is very similar Riemann problem with the exact solution. But in the contact part of the relatively large difference in the end, we also use Test 1 of the initial conditions, simulated a different Knudsen number, from 1 to $1 \text{ E-}20$, showed that when the Knudsen number close to zero, results will be close Riemann problem of the exact solution. The future, we hope that we can use CESE Method, and the combination of Model Boltzmann equation and the Navier-Stork equation to simulate Shock wave problems.



致謝

有人說，致謝是整各碩士論文中，最難寫的一章，我想困難點可能就是因為要在有限的篇幅中，表達出心中內心的感動與感謝。此時，我有深刻的體驗。兩年的光陰，速度快到我渾然不覺，還在驚訝中，人生就到了新的開端。在交大的兩年中，遭遇的事情，每件都是直得一再回味與思考。有喜有悲，有對有錯，每種心情都是我成長的元素。

在論文付梓之際，心中滿是感謝。感謝上天的安排，讓我在交通大學度過美好與充實的歲月，匯聚如此之因緣。本論文得以順利之完成，首先要感謝指導教授 吳宗信 教授在論文撰寫期間之督促與悉心指導，在遭遇瓶頸時總是幫我渡過難關，解決心中的疑問，恩師在研究工作上的積極與執著態度，是我學習的榜樣，本人由衷感謝指導老師吳宗信 教授在本人求學期間所給予的殷切指導。

在這段學習成長的期間感謝所有陪伴我同甘共苦的夥伴，洪維呈、林宗漢、陳又寧、謝昇汎等已畢業的學長與我分享學術上的心得，以及APPL實驗室的學長姐，洪捷榮、胡孟樺、邱沅明、江明鴻、林雅茹、李允民、鄭凱文、林昆模、周欣芸、李富利等，在各方面的幫忙與協助，以及同儕柳志良、劉育宗、鄭丞志、呂政霖、林士傑、蘇正勤等，平時在課業與實驗心得之交流，與你們努力奮鬥相處的時光將是我最美好的回憶，也感謝碩一的學弟，穎志、必任、逸民、俊傑等

學弟的協助與鼓勵，使我的人生增添了許多美好的歡笑與回憶以及來自紐西蘭的Hadley M. Cave (瓦片)和法國的ALIAT Abdelaziz，使我這兩年過得相當充實且溫馨，並能順利完成學業。

另外還要特別感謝男友竹昇，在本論文寫作期間給予的鼓勵與幫助，最重要的我要感謝永遠默默付出的家人之關懷與鼓勵，特別是我的父母、二妹、三妹，四弟對我的包容，讓我得以無憂無慮的求學，由於有他們精神與生活上的支持與鼓勵，我才能順利完成學業。



吳玟琪 謹誌于

風城交大

中華民國九十七年七月

Table of Contents

摘要.....	I
Abstrac	II
致謝.....	IV
Table of Contents	VI
List of Tables.....	VII
List of Figures	VIII
Nomenclature.....	X
Chapter 1 Introduction	1
1.1 Background and Motivation	1
1.2 Literature Review.....	2
1.3 Specific Objectives of the Thesis Study	2
Chapter 2 The Space-Time CESE Method for 1-D Continuum Flow Equation	3
2.1 The a Scheme	3
2.2 The c Scheme	7
2.3 Euler Equation and the a- ϵ Scheme	7
Chapter 3 The Space-Time CESE Method for 1D Kinetic Model Boltzmann Equation	14
3.1 BGK Model Boltzmann Equation.....	14
3.1.1 Kinetic model Boltzmann equations.....	14
3.1.2 Nondimensionalization	17
3.2 Discretization of model Boltzmann Equation.....	19
3.2.1 Spatial Discretization Using The a- ϵ - α - β Scheme	19
3.2.2 Velocity Discretization Using Discrete Ordinate Method.....	21
3.2.3 Treatment of Source Terms	22
Chapter 4 Results and Discussions	24
4.1 Overview.....	24
4.2 Results of the Euler Equation Using the CESE Model.....	24
4.3 Results of the Model Boltzmann Using the CESE Model.....	25
Chapter 5 Conclusion.....	26
5.1 Summery	26
5.2 Recommendations for Future work	26
References:.....	27

List of Tables

Table 1 Initial conditions for five test problems.28



List of Figures

Fig. 1. The SEs and CEs of type : (a) The relative of SEs and CEs; (b) SEs(j,n); (c) CE-(j,n); (d) CE+(j,n) ,Source S. C. Chang [1995] J. C. P	29
Fig.2 Test 1 Exact solution for density, velocity, pressure, and temperature at time t = 0.25 s	30
Fig.3 Test 2 Exact solution for density, velocity, pressure, and temperature at time t = 0.012 s	31
Fig.4 Test 3 Exact solution for density, velocity, pressure, and temperature at time t = 0.012 s	32
Fig.5 Test 4 Exact solution for density, velocity, pressure, and temperature at time t = 0.15 s	33
Fig.6 Test 5 Exact solution for density, velocity, pressure, and temperature at time t = 0.25 s	34
Fig.7 Test 1: The numerical results when t=0.001s	35
Fig.8 Test 1: The numerical results when t=0.1s	36
Fig.9 Test 1: The numerical results when t=0.2s	37
Fig.10 Test 1: The numerical results when t=0.3s	38
Fig.11 Test 1: The numerical results when t=0.6s	39
Fig.12 Test 2: The numerical results when t=0.001s	40
Fig.13 Test 2: The numerical results when t=0.03s	41
Fig.14 Test 2: The numerical results when t=0.17s	42
Fig.15 Test 2: The numerical results when t=0.23s	43
Fig.16 Test 3: The numerical results when t=0.001s	44
Fig.17 Test 3: The numerical results when t=0.3s	45
Fig.18 Test 3: The numerical results when t=0.17s	46
Fig.19 Test 3: The numerical results when t=0.23s	47
Fig.20 Test 4: The numerical results when t=0.001s	48
Fig.21 Test 4: The numerical results when t=0.035s	49
Fig.22 Test 4: The numerical results when t=0.095s	50
Fig.23 Test 4: The numerical results when t=0.2s	51
Fig.24 Test 5: The numerical results when t=0.0001s	52
Fig.25 Test 5: The numerical results when t=0.0035s	53
Fig.26 Test 5: The numerical results when t=0.02s	54
Fig.27 Test 5: The numerical results when t=0.04s	55
Fig.28 Test 1: Simulation of density in different Knudsen number of results when t = 0.2s	56
Fig.29 Test 1: Simulation of pressure in different Knudsen number of results when t =	

0.2s.....57
Fig.30 Test 1: Simulation of temperature in different Knudsen number of results when
t = 0.2s.....58
Fig.31 Test 1: Simulation of velocity in different Knudsen number of results when t =
0.2s.....59



Nomenclature

ν :the elastic collision frequency

n :number density

k :Boltzmann constant

μ :viscosity

P_r :Prandtl number

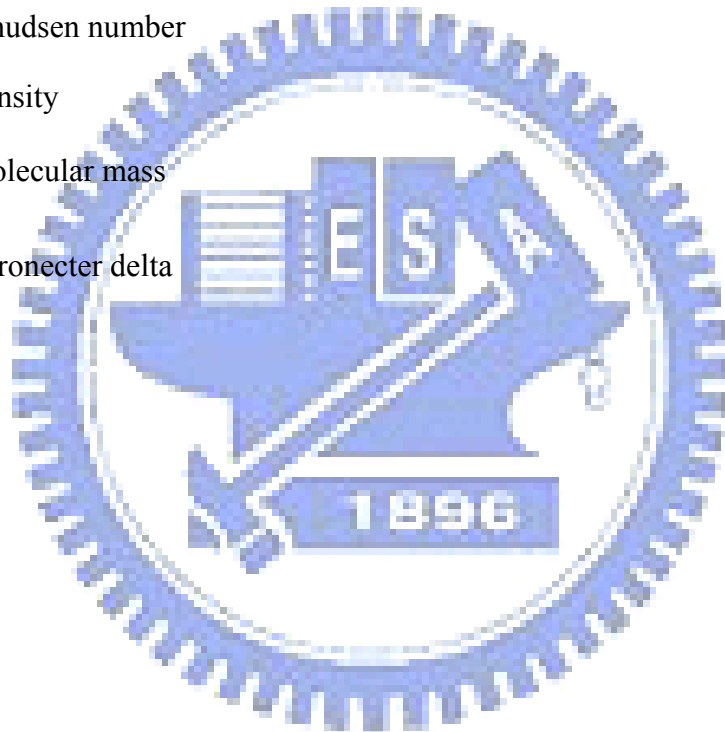
λ :mean free path

Kn :Knudsen number

ρ :density

m :molecular mass

δ_{ij} :Kronecker delta



Chapter 1 Introduction

1.1 Background and Motivation

Fluid dynamics is one of fields in which computer simulation shows a great deal of promise, and interest in the development of better algorithms. Usually, continuum methods fail in continuum breakdown region where non-equilibrium and rarefaction are strong. So continuum methods can not use in all flow fields condition. In the direct simulation Monte Carlo (DSMC) method provides physical accuracy but its computational cost is extremely high in relatively high density regions. In this situation, we find a new numerical simulation method. The method of space- time conservation element and solution element (CESE) is a new numerical framework for solving Model Boltzmann Equation (MBE). It is the method which proposed by Sin-Chung Chang from 1991 to the present. The CESE method, it has advantage: (1) it is explicit scheme, and differs the traditional numerical method. (2) High accuracy in capturing discontinuity, (3)good performance in non-reflecting boundary condition treatment, Moreover, it is capable of generating accurate shock tube solutions with the CFL number ranging from close to 1 to 0.022. We objective is to develop a 1-D of MBE-Euler solver using the CESE method.

1.2 Literature Review

[1] proposed a CESE method, and integrity explains the CESE method in 1995. It introduced the a - ε scheme apply the Euler equation in this article. A summary of the key results of the present method work has been given. Behind these results is a continuous effort to maintain the simplicity, generality, and accuracy of the present method. [2] proposed CESE method for treatment of stiff source terms in 1997. Using CESE method dispose of stiff source terms and non-stiff source terms problems. [3] proposed hyperbolic systems with stiff and non stiff source terms in CESE method. At present, only one dimension and two dimension or three dimension has not been reported .

1.3 Specific Objectives of the Thesis Study

Based on previous reviews, the objectives of the current study are summarized as follow.

1. To develop of MBE solver using the CESE method.
2. To apply the MBE method to 1-D shock problems
3. Compared with different Knudsen number result.

Chapter2 The Space-Time CESE Method for 1-D Continuum Flow Equation

2.1 The a Scheme

In this section, we consider a hyperbolic equation.

$$\frac{\partial u}{\partial t} + a \frac{\partial u}{\partial x} = 0 \tag{2.1.1}$$

Let $x_1 = x$ and $x_2 = t$ be the coordinates of a 2D Euclidean space E_2 . Because

Eq. (2.1.1)

$$\nabla \cdot \vec{h} = \frac{\partial (au)}{\partial x} + \frac{\partial u}{\partial t} = 0 \tag{2.1.2}$$

Gauss' divergence theorem

$$\oint_{S(V)} \vec{h} \cdot d\vec{s} = 0 \tag{2.1.3}$$

Here

$$d\vec{s} = d\sigma \vec{n} \text{ and } \vec{h} = (au, u) \tag{2.1.4}$$

with (i) $S(V)$ being the boundary of a space-time region V in E_2 ; and (ii) $d\sigma$ and \vec{n} being the area and the outward unit normal of a surface element on $S(V)$.

At this juncture, note that the conservation law give in Eq.(2.1.3) is formulated in a form in which space and time are unified and treated on the same footing. This unity of space and time is also a tenet in the following numerical development. It is a key characteristic that distinguishes the present method from most of the traditional

methods.

Let Ω denote the set of mesh points (j, n) in E_2 (dots in Fig. 1(a)), where $n = 0, \pm \frac{1}{2}, \pm 1, \pm \frac{3}{2}, \pm 2, \pm \frac{5}{2}, \dots$, and, for each $n, j = n \pm \frac{1}{2}, n \pm \frac{3}{2}, n \pm \frac{5}{2}, \dots$. There is a solution element (SE) associated with each $(j, n) \in \Omega$. Let the solution SE (j, n) be the interior of the space-time region boundary by a dashed curve depicted in Fig. 1(b). It includes a horizontal line segment, a vertical line segment, and their immediate neighborhood does not matter.

Let E_2 be divided into no overlapping rectangular regions (see Fig.1(a)) referred to as conservation element (CEs). As depicted in Figs. 1(c) and 1(d), the CE with its top-right (top-left) vertex being the mesh point $(j, n) \in \Omega$ is denoted by $CE_-(j, n)$ ($CE_+(j, n)$). Obviously the boundary of $CE_-(j, n)$ ($CE_+(j, n)$), excluding two isolated point B and C (C and D), is formed by the subsets of $SE(j, n)$ and $SE(j-1/2, n-1/2)$ ($SE(j+1/2, n-1/2)$). The current approximation of Eq.(2.1.3) is

$$F_{\pm} \stackrel{def}{=} \oint_{S(CE_{\pm}(j, n))} \vec{h} \cdot d\vec{s} = 0 \quad (2.1.5)$$

For any $(j, n) \in \Omega$, Let

$$u(x, t) \approx u^*(x, t; j, n) \text{ and } \vec{h}(x, t) \approx \vec{h}^*(x, t; j, n) \quad (2.1.6)$$

with

$$u^*(x, t; j, n) \stackrel{def}{=} u_j^n + (u_x)_j^n (x - x_j) + (u_t)_j^n (t - t^n) \quad (2.1.7)$$

$$\vec{h}^*(x, t; j, n) \stackrel{def}{=} (a u^*(x, t; j, n), u^*(x, t; j, n)) \quad (2.1.8)$$

Here (i) $u_j^n, (u_x)_j^n$, and $(u_t)_j^n$ are constants in $SE(j, n)$; and (ii) $x_j = j\Delta x$ and $t^n = n\Delta t$.

Let $u = u(x, t; j, n)$ satisfy Eq. (2.1.1). Then

$$(u_t)_j^n = -a(u_x)_j^n \quad (2.1.9)$$

Eqs. (2.1.7) and (2.1.9)

$$u^* = u(x, t; j, n) = u_j^n + (u_x)_j^n [(x - x_j) - a(t - t^n)] \quad (x, t) \in SE(j, n) \quad (2.1.10)$$

This condition can be used to simplify evaluation of the flux across a simple curve that lies entirely within an SE. According to the top expression given in Eq.(2.1.2),

$\Delta h = 0$ implies that there exists a function $\psi^*(x, t; j, n)$ such that

$$(u_t)_j^n = -a(u_x)_j^n \quad (2.1.11)$$

$$\frac{\partial \psi(x, t; j, n)}{\partial t} = au^*(x, t; j, n) \quad (2.1.12)$$

And

$$-\frac{\partial \psi(x, t; j, n)}{\partial x} = u^*(x, t; j, n) \quad (2.1.13)$$

for any $(x, t) \in SE(j, n)$. Substituting Eq.(2.1.11) and Eq.(2.1.12), one concludes that,

up to an arbitrary constant,

$$\psi(x, t; j, n) = -\left[(x - x_j) - a(t - t^n)\right]^2 \frac{(u_x)_j^n}{2} - \left[(x - x_j) - a(t - t^n)\right] u_j^n \quad (2.1.14)$$

Let $(x, t) \in SE(j, n)$ and $(x', t') \in SE(j, n)$. Let Γ be a simple curve joining (x, t) and (x', t') , and lying entirely within $SE(j, n)$

$$\int_{\Gamma} h^* \cdot ds = \psi(x', t'; j, n) - \psi(x, t; j, n) \quad (2.1.15)$$

Here we assume that ds points to the right of Γ if one moves forward from (x, t) to (x', t') . Eq.(2.1.14) states that the flux of h^* across the curve Γ is give by the difference in the values of ψ at its two end-points. This reason, $\psi(x, t; j, n)$ will be referred to as the potential function associated with SE(j, n).

Let

$$(u_x^-)_j^n \stackrel{def}{=} \frac{\Delta x}{2} (u_x)_j^n \text{ and } \nu \stackrel{def}{=} \frac{a\Delta t}{\Delta x} \quad (2.1.16)$$

Because

$$\frac{\partial u}{\partial x} = \frac{\Delta x}{2} \frac{\partial u}{\partial x} \quad \text{if } x = \frac{\Delta x}{2} \quad (2.1.17)$$

The $(u_x^-)_j^n$ is a numerical analogue of $\partial u / \partial x$ at (j, n) . Using Eq.(2.1.14)

$$\oint_{S(CE_+(j,n+1))} \vec{h} \cdot d\vec{s} = 0 \quad (j, n+1) \in \Omega \quad (2.1.18)$$

and

$$\oint_{S(CE_-(j,n+1))} \vec{h} \cdot d\vec{s} = 0 \quad (j, n+1) \in \Omega \quad (2.1.19)$$

Obtains

$$(1-\nu)[u + (1+\nu)u_x^-]_j^{n+1} = (1-\nu)[u - (1+\nu)u_x^-]_{j+1}^n \quad (2.1.20)$$

respective

$$(1+\nu)[u - (1-\nu)u_x^-]_j^{n+1} = (1+\nu)[u + (1-\nu)u_x^-]_{j-1}^n \quad (2.1.21)$$

The basic form \Leftrightarrow the for ward marching form of the α scheme, i.e.,

$$u_j^{n+1} = \frac{1}{2} \left\{ (1-\nu)[u - (1+\nu)u_x^-]_{j+1}^n + (1+\nu)[u + (1-\nu)u_x^-]_{j-1}^n \right\} \quad (2.1.22)$$

$$(u_x^-)_j^{n+1} = \frac{1}{2} \left\{ [u - (1+\nu)u_x^-]_{j+1}^n - [u + (1-\nu)u_x^-]_{j-1}^n \right\} \quad (2.1.23)$$

2.2 The c Scheme

Let

$$u'_{j\pm 1/2}{}^n \stackrel{def}{=} u_{j\pm 1/2}^{n-1/2} + (\Delta t/2)(u_t)_{j\pm 1/2}^{n-1/2} \quad (2.2.1)$$

Using $(u_t)_j^n = -a(u_x)_j^n$ and $\nu = a\Delta t / \Delta x$, we can obtain

$$u'_{j\pm 1/2}{}^n = [u - 2\nu u_{\bar{x}}]_{j\pm 1/2}^{n-1/2} \quad (2.2.2)$$

Because $u'_{j\pm 1/2}{}^n$ is a first-order Taylor's approximation of u at $(j\pm 1/2, n)$,

$$(u_{\bar{x}}^c)_j^n \stackrel{ddef}{=} \frac{\Delta x}{4} \left(\frac{u'_{j+1/2}{}^n - u'_{j-1/2}{}^n}{\Delta x} \right) = \frac{u'_{j+1/2}{}^n - u'_{j-1/2}{}^n}{4} \quad (2.2.3)$$

is a central-differential analogue of $\partial u / \partial \bar{x}$ at (j, n) . The c scheme is formed by

$$u_j^n = \frac{1}{2} \left\{ (1-\nu) [u - (1+\nu)u_{\bar{x}}]_{j+1/2}^{n-1/2} + (1+\nu) [u + (1-\nu)u_{\bar{x}}]_{j-1/2}^{n-1/2} \right\} \quad (2.2.4)$$

and

$$(u_x)_j^n = (u_{\bar{x}}^c)_j^n \quad (2.2.5)$$

2.3 Euler Equation and the a-ε Scheme

The α - ε scheme is formed by

$$u_j^n = \frac{1}{2} \left\{ (1-\nu) [u - (1+\nu)u_x]_{j+1/2}^{n-1/2} + (1+\nu) [u + (1-\nu)u_x]_{j-1/2}^{n-1/2} \right\} \quad (2.3.1)$$

and

$$(u_x)_j^n = (1-2\varepsilon)(u_x^a)_j^n + 2\varepsilon(u_x^c)_j^n \quad (2.3.2)$$

and

$$\left(u_x^a\right)_j^{n+1} = \frac{1}{2} \left\{ \left[u - (1+v)u_x^- \right]_{j+1}^n - \left[u + (1-v)u_x^- \right]_{j-1}^n \right\} \quad (2.3.3)$$

$$\left(u_x^c\right)_j^n = \frac{\Delta x}{4} \left(\frac{u_{j+1/2}^n - u_{j-1/2}^n}{\Delta x} \right) = \left(\frac{u_{j+1/2}^n - u_{j-1/2}^n}{4} \right) \quad (2.3.4)$$

$$u_{j\pm 1/2}^n = u_{j\pm 1/2}^{n-1/2} + (\Delta t / 2)(u_t)_{j\pm 1/2}^{n-1/2}$$

Thus the α - ε scheme reduces to the α scheme when $\varepsilon=0$.

We consider a dimensionless form of the 1D unsteady Euler equations of a perfect gas. Let ρ, v, p and γ be the mass, density, velocity, static pressure, and constant specific heat ratio, respectively. Let

$$u_1 = \rho \quad u_2 = \rho v \quad u_3 = p / (\gamma - 1) + \left(\frac{1}{2}\right) \rho v^2 \quad (2.3.5)$$

$$f_1 = u_2 \quad (2.3.6)$$

$$f_2 = (\gamma - 1)u_3 + \left(\frac{1}{2}\right)(3 - \gamma)(u_2)^2 / (u_1) \quad (2.3.7)$$

and

$$f_3 = \gamma u_2 u_3 / u_1 - \left(\frac{1}{2}\right)(\gamma - 1)(u_2)^3 / (u_1)^2 \quad (2.3.8)$$

Then the Euler equations can be expressed as

$$\frac{\partial u_m}{\partial t} + \frac{\partial f_m}{\partial x} = 0 \quad m = 1, 2, 3 \quad (2.3.9)$$

The integral form of Eq. (2.1.15) in space-time E_2 is

$$\oint_{S(v)} \bar{h} \cdot d\bar{s} = 0 \quad m = 1, 2, 3 \quad (2.3.10)$$

Where $h_m = (f_m, u_m)$, $m = 1, 2, 3$, are the space-time mass, momentum, and energy current density vectors, respectively.

As a preliminary, let

$$f_{m,k} \stackrel{def}{=} \partial f_m / \partial u_k \quad m = 1,2,3 \quad (2.3.11)$$

Consider SEs. For any $(x,t) \in SE(x,t)$, $u_m(x,t)$, $f_m(x,t)$, and $h_m(x,t)$ are approximated by $u_m^*(x,t;j,n)$, $f_m^*(x,t;j,n)$, and $h_m^*(x,t;j,n)$, respectively. They will be defined shortly. Let

$$u_m^*(x,t;j,n) \stackrel{def}{=} (u_m)_j^n + (u_{mx})_j^n (x - x_j) + (u_{mt})_j^n (t - t^n) \quad (2.3.12)$$

Where $(u_m)_j^n$, $(u_{mx})_j^n$, and $(u_{mt})_j^n$ are constants in $SE(j,n)$. Obviously, they can be considered as the numerical analogues of the values of u_m , $\partial u_m / \partial x$, and $\partial u_m / \partial t$ at (x_m, t^n) , respectively.

Let $(f_m)_j^n$ and $(f_{m,k})_j^n$ denote the values of f_m and $f_{m,k}$, respectively, when u_m , $m = 1,2,3$, respectively, assume the values of $(u_m)_j^n$, $m = 1,2,3$. Let

$$(f_{mx})_j^n \stackrel{def}{=} \sum_{k=1}^3 (f_{m,k})_j^n (u_{kx})_j^n \quad (2.3.13)$$

And

$$(f_{mt})_j^n \stackrel{def}{=} \sum_{k=1}^3 (f_{m,k})_j^n (u_{kt})_j^n \quad m = 1,2,3 \quad (2.3.14)$$

Because

$$\frac{\partial f_m}{\partial x} = \sum_{k=1}^3 f_{m,k} \frac{\partial u_k}{\partial x} \quad (2.3.15)$$

And

$$\frac{\partial f_m}{\partial t} = \sum_{k=1}^3 f_{m,k} \frac{\partial u_k}{\partial t} \quad (2.3.16)$$

$(f_{mx})_j^n$ and $(f_{mt})_j^n$ can be considered as the numerical analogues of the values of $\partial f_m / \partial x$ and $\partial f_m / \partial t$ at (x_m, t^n) , respectively. As a result, we assume that

$$f_m^*(x, t; j, n) = (f_m)_j^n + (f_{mx})_j^n (x - x_j) + (f_{mt})_j^n (t - t^n) \quad m=1,2,3 \quad (2.3.17)$$

Because $h_m = (f_m, u_m)$, we also assume that

$$h_m^*(x, t; j, n) = (f_m^*(x, t; j, n), u_m^*(x, t; j, n)) \quad (2.3.18)$$

Moreover, we assume that, for any $(x, t) \in \text{SE}(j, n)$, $u_m = u_m^*(x, t; j, n)$ and

$f_m = f_m^*(x, t; j, n)$, satisfy Eq.(2.3.9)

$$\frac{\partial u_m^*(x, t; j, n)}{\partial t} + \frac{\partial f_m^*(x, t; j, n)}{\partial x} = 0 \quad (2.3.19)$$

According to Eq. (2.3.12) and (2.3.17), Eq. (2.3.19) is equivalent to

$$(u_{mt})_j^n = -f_m (u_{mx})_j^n \quad (2.3.20)$$

Because $(f_{mx})_j^n$ are function of $(u_m)_j^n$ and $(u_{mx})_j^n$, Eq.(2.40) implies that $(u_{mt})_j^n$ are also functions of $(u_m)_j^n$ and $(u_{mx})_j^n$. From this result and the facts stated following Eq. (2.3.18), one concludes that the only independent discrete variables needed to be solved in the current marching scheme are $(u_m)_j^n$ and $(u_{mx})_j^n$.

From Eq.(2.3.19), one concludes that the generalization of the potential function $\psi(x, t; j, n)$, $m = 1, 2, 3$, which satisfy

$$\frac{\partial \psi_m(x, t; j, n)}{\partial t} = f_m^*(x, t; j, n) \quad (2.3.21)$$

and

$$-\frac{\partial \psi_m(x, t; j, n)}{\partial x} = u_m^*(x, t; j, n) \quad (2.3.22)$$

Substituting Eq.(2.3.12) and (2.3.17) into Eq. (2.3.21) and Eq.(2.3.22), and using

Eq.(2.3.20), one concludes that , up to an arbitrary constant,

$$\begin{aligned} \psi_m(x, t; j, n) &= (f_m)_j^n (t - t^n) - (u_m)_j^n (x - x_j) + \left(\frac{1}{2}\right) (f_{mt})_j^n (t - t^n)^2 \\ &\quad - \left(\frac{1}{2}\right) (u_{mx})_j^n (x - x_j)^2 + (f_{mx})_j^n (x - x_j) (t - t^n) \end{aligned} \quad (2.3.23)$$

by using an argument similar to that leading to Eq.(2.1.15), Here Γ is simple curve joining (x, t) and (x', t') , and lying entirely within $SE(j, n)$. We also assume that ds points to the right of Γ if one moves forward from (x, t) to (x', t') .

As in the α - ε scheme, we assume that the flux of h_m^* is conserved over $CE(j, n)$,

$$\int_{S(CE(j,n))} h_m^* \cdot ds = 0 \quad (2.3.24)$$

Combining Eq. (2.3.23) and (2.3.24), one has

$$\begin{aligned} &\psi_m(x_j - \Delta x/2, t^n; j, n) - \psi_m(x_j + \Delta x/2, t^n; j, n) \\ &+ \psi_m(x_{j+1/2}, t^{n-1/2} + \Delta t/2; j+1/2, n-1/2) \\ &- \psi_m(x_{j+1/2} - \Delta x/2, t^{n-1/2} + \Delta t/2; j+1/2, n-1/2) \\ &+ \psi_m(x_{j-1/2} + \Delta x/2, t^{n-1/2}; j-1/2, n-1/2) \\ &- \psi_m(x_{j-1/2}, t^{n-1/2} + \Delta t/2; j-1/2, n-1/2) = 0 \end{aligned} \quad (2.3.25)$$

Substitution of Eq.(2.3.23) and (2.3.25)

$$(u_m)_j^n = \frac{1}{2} \left[(u_m)_{j-1/2}^{n-1/2} + (u_m)_{j+1/2}^{n-1/2} + (s_m)_{j-1/2}^{n-1/2} - (s_m)_{j+1/2}^{n-1/2} \right] \quad (2.3.26)$$

where, for all $(j, n) \in \Omega$,

$$(s_m)_j^n = \frac{\Delta x}{4} (u_{mx})_j^n + \frac{\Delta t}{\Delta x} (f_m)_j^n + \frac{(\Delta t)^2}{4\Delta x} (f_{mt})_j^n \quad (2.3.27)$$

And

$$(u_{mx})_j^n = \left[(u'_m)_{j+1/2}^n - (u'_m)_{j-1/2}^n \right] / \Delta x + (2\varepsilon - 1) (du_{mx})_j^n \quad (2.3.28)$$

$$(u'_m)_{j\pm 1/2}^n = (u_m)_{j\pm 1/2}^{n-1/2} + (\Delta t/2) (u_{mt})_{j\pm 1/2}^{n-1/2} \quad (2.3.29)$$

$$(du_{mx})_j^n = \frac{1}{2} \left[(u_{mx})_{j+1/2}^{n-1/2} + (u_{mx})_{j-1/2}^{n-1/2} \right] - \left[(u_m)_{j+1/2}^{n-1/2} - (u_m)_{j-1/2}^{n-1/2} \right] / \Delta x \quad (2.3.30)$$

where ε is a parameter independent of numerical variables. Note that the last term, vanishes if $\varepsilon=1/2$.

We conclude this section by introducing some possible modification to the above solver. Note that $(u'_m)_{j\pm 1/2}^n$, by its definition, represents a finite-difference approximation of u_m at $(j\pm 1/2, n)$.

As a result,

$$(u_{mx}^c)_j^n = [(u'_m)_{j+1/2}^n - (u'_m)_{j-1/2}^n] / \Delta x \quad (2.3.31)$$

Respectively, are the central-difference approximations for $\partial u_m / \partial x$, the above central-difference approximation is valid as long as no discontinuity of u_m occurs between $(j-1/2, n)$ and $(j+1/2, n)$. In the following discussion, we develop alternates which are valid even in the presence of discontinuity.

Let

$$(u_{mx+})_j^n = \left\{ \frac{(u_m)_{j+1/2}^{n-1/2} + (\Delta t / 2)(u_m)_{j+1/2}^{n-1/2} - (u_m)_j^n}{\Delta x / 2} \right\} \quad (2.3.32)$$

$$(u_{mx-})_j^n = \left\{ \frac{(u_m)_j^n - (u_m)_{j-1/2}^{n-1/2} + (\Delta t / 2)(u_m)_{j-1/2}^{n-1/2}}{\Delta x / 2} \right\} \quad (2.3.33)$$

can be obtained

$$(u_{mx}^c)_j^n = \frac{1}{2} [(u_{mx-})_j^n + (u_{mx+})_j^n] \quad (2.3.34)$$

As a result of the above considerations, $(u_{mx}^c)_j^n$ can be replaced by

$$(u_{mx}^{w_0}) = w_0 \left((u_{mx-})_j^n, (u_{mx+})_j^n; \alpha \right) \quad m = 1, 2, 3 \quad (2.3.35)$$

Here α is an adjustable constant and the function w_0 is defined by (i)

$w_0(0,0,\alpha) = 0$ and (ii)

$$w_0\left((x_-)_j^n, (x_+)_j^n; \alpha\right) = \frac{|x_+|^\alpha x_- + |x_-|^\alpha x_+}{|x_+|^\alpha + |x_-|^\alpha} \quad (|x_+| + |x_-| > 0) \quad (2.3.36)$$

For $\alpha > 0$, this average is biased toward the one among x_+ and x_- with the smaller magnitude. For the same value of $|x_+|$ and $|x_-|$, the bias increases as α increases.

Thus, we always chose $\alpha \geq 0$.



Chapter 3 The Space-Time CESE Method for 1D Kinetic Model Boltzmann Equation

3.1 BGK Model Boltzmann Equation

3.1.1 Kinetic model Boltzmann equations

Assume there is no external force. we consider a class of model Boltzmann equations of the form

$$\frac{\partial f}{\partial t} + v \cdot \frac{\partial f}{\partial x} = C(f) \quad (3.1.1)$$

For BGK (Bhatnagar-Gross-Krook) model, the collision integral term $C(f)$ is modeled by the relaxation off toward the Maxwellian equilibrium distribution $M[f]$.

The collision operator is now

$$C(f) = \nu(M[f] - f) \quad (3.1.2)$$

According to the Chapman-Enskog solution to the BGK equation, the elastic collision frequency is the form

$$\nu = \frac{nkT}{\mu} \quad (3.1.3)$$

where T is temperature. n is number density. k is the Boltzmann constant and μ is the viscosity assumed temperature dependence

$$\frac{\mu}{\mu_{ref}} = \left(\frac{T}{T_{ref}} \right)^\chi \quad (3.1.4)$$

the subscript *ref* states the reference condition of the temperature viscosity power law. The power χ is constant for a given gas. If we assume the dependence of the viscosity on the temperature as for the Chapman-Cowling gas of inverse ζ power law we have

$$\chi = \frac{\zeta + 3}{2(\zeta - 1)} \quad (3.1.5)$$

For Maxwellian molecules. $\zeta = 5$ then $\chi = 1$; thus the collision frequency is independent of temperature. The viscosity coefficient at free stream state μ_∞ is relate to the free stream mean free path λ_∞ by the relation

$$\mu_\infty = \frac{5}{16} mn_\infty (2\pi RT_\infty)^{1/2} \lambda_\infty \quad (3.1.6)$$

The local Maxwellian equilibrium distribution function given by

$$M[f] = n \left(\frac{1}{2\pi RT} \right)^{3/2} \exp \left\{ -\frac{1}{2RT} [(v_x - u_x)^2] \right\} \quad (3.1.7)$$

Since the work of Bhatnagar, Gross and Krook, there are several other nonlinear model Boltzmann equations have been proposed. These include the ellipsoidal model by Hoiway and by Cercignam & Taoni, the polynomial and triode gain function models by Segal & Femger, and the one by Shakov and by Abe & Oguchi. The latter three used rather systematic procedures to construct model equations for the nonlinear

Boltzmann equation. For Shakov model, we have

$$C(f) = v(s[f] - f) \quad (3.1.8)$$

where $S[f]$ defined as

$$S[f] = M[f] \left[1 + (1 - \text{Pr}) c \cdot q \left(\frac{c^2}{RT} - 5 \right) / (5pRT) \right] \quad (3.1.9)$$

Here. Pr is the Prandtl number and is equal 2/3 for a monotonic gas. The number density n , flow velocity u_i , and temperature T of the gas are the first three moments of the distribution function

$$n(x, t) = \int f(x, v, t) d^3v \quad (3.1.10)$$

$$nu_i(x, t) = \int v_i f(x, v, t) d^3v \quad (3.1.11)$$

$$\frac{3}{2} nRT(x, t) = \frac{1}{2} \int c^2 f(x, v, t) d^3v \quad (3.1.12)$$

R is the gas constant. $c = v - u(x, t)$ is the peculiar velocity of the molecule. It is convenient to introduce also the following higher order moments defined by

$$P_{ij}(x, t) = \int c_i c_j f(x, v, t) d^3v \quad (3.1.13)$$

$$S_{ijk}(x, t) = \int c_i c_j c_k f(x, v, t) d^3v \quad (3.1.14)$$

Then the gas pressure p and stress tensor τ_{ij} are

$$p(x, t) = \frac{1}{3} m P_{ii} \quad (3.1.15)$$

$$\tau_{ij}(x, t) = m P_{ij} - p \delta_{ij} \quad (3.1.16)$$

The equation of status also can be proved by the definitions of pressure and temperature. That is

$$p(x, t) = \rho RT = nmRT = n(x, t)kT(x, t) \quad (3.1.17)$$

where ρ is the density, m is molecular mass and $mR = k$. k is the Boltzmann constant and δ_{ij} is the Kronecker delta. The heat flux vector q is

$$q_i(x, t) = \frac{1}{2} m S_{ij} = \frac{1}{2} m \int c_i c_j f(x, v, t) d^3v \quad (3.1.18)$$

The kinetic energy of monotonic gas associated with thermal or translation motion is

$$e(x, t) = \frac{3}{2} kT(x, t) = \frac{1}{2} m \int c^2 f(x, v, t) d^3v \quad (3.1.19)$$

3.1.2 Nondimensionalization

A characteristic velocity C_∞ and time t_∞ can be defined

$$C_\infty = \sqrt{2RT}, t_\infty = L/C_\infty \quad (3.1.20)$$

where L is a characteristic length, T_∞ is the reference temperature of the problem.

The definitions of nondimensional variables are introduced as

$$\begin{aligned} \hat{t} &= t/t_\infty, \hat{x} = x/L, \hat{f} = f/(n_\infty/C_\infty^3), \\ \hat{n} &= n/n_\infty, \hat{T} = T/T_\infty, \hat{p} = p/p_\infty, \\ \hat{u} &= u/C_\infty, \hat{v} = v/C_\infty, \hat{q} = q/q_\infty, \\ \hat{\tau}_{ij} &= \tau_{ij}/mn_\infty C_\infty^2 \end{aligned} \quad (3.1.21)$$

The reference pressure p_∞ and heat flux q_∞ can be defined with primitive reference variables n_∞ , T_∞ , and C_∞ by

$$p_\infty = \frac{1}{2} mn_\infty C_\infty^2$$

$$q_\infty = \frac{1}{2} mn_\infty C_\infty^3$$
(3.1.22)

Without causing any confusion we shall drop the hat in the equations in the following.

The nondimensional kinetic model equation is written as

$$\frac{\partial f}{\partial t} + v \cdot \frac{\partial f}{\partial x} = \nu (f^+ - f)$$
(3.1.23)

where $f^+ = M[f]$ for BGK model equation.,

$$M[f] = \frac{n}{(\pi T)^{3/2}} \exp\left(-\frac{c^2}{T}\right)$$
(3.1.24)

The macroscopic moments are found as

$$n = \int_{-\infty}^{\infty} \int_{-\infty}^{\infty} \int_{-\infty}^{\infty} f dv_x dv_y dv_z$$
(3.1.25)

$$v = \int_{-\infty}^{\infty} \int_{-\infty}^{\infty} \int_{-\infty}^{\infty} v f dv_x dv_y dv_z$$
(3.1.26)

$$\frac{3}{2} nT = \int_{-\infty}^{\infty} \int_{-\infty}^{\infty} \int_{-\infty}^{\infty} c^2 f dv_x dv_y dv_z$$
(3.1.27)

$$p = nT$$
(3.1.28)

$$\tau_{ij}(x, t) = \int_{-\infty}^{\infty} \int_{-\infty}^{\infty} \int_{-\infty}^{\infty} c_i c_j f dv_x dv_y dv_z - \frac{1}{2} p \delta_{ij}$$
(3.1.29)

$$q = \int_{-\infty}^{\infty} \int_{-\infty}^{\infty} \int_{-\infty}^{\infty} c c^2 f dv_x dv_y dv_z$$
(3.1.30)

The nondimensional collision frequency for gas of inverse power law is of the form

$$\nu = \frac{8nT^{1-\chi}}{5\sqrt{\pi}Kn_\infty}$$
(3.1.31)

Where $Kn_\infty = \lambda_\infty / L$ is the Knudsen number of reference status. λ_∞ is the mean free path of reference status: can be defined by hard sphere molecular model as

$$\lambda_\infty = \frac{16\mu_\infty}{5n_\infty m \sqrt{2\pi RT_\infty}} \quad (3.1.32)$$

and the power $1 - \chi = (\zeta - 5) / [2(\zeta - 1)]$. For Maxwell molecules, $\zeta = 5$ then $1 - \chi = 0$;

$$\nu = \frac{8n}{5\sqrt{\pi} Kn_\infty} \quad (3.1.33)$$

the collision frequency is independent of temperature. The average collision time of reference status is

$$\tau_\infty = \frac{\lambda}{C_\infty} = \frac{4\mu_\infty}{5p_\infty} \quad (3.1.34)$$

Where $\bar{C}_\infty = 2C_\infty / \sqrt{\pi}$ is average peculiar velocity. The local mean free path and average local collision time are

$$\frac{\lambda}{\lambda_\infty} = \frac{T^{\chi-1/2}}{n} \quad \frac{\tau}{\tau_\infty} = \frac{\mu}{p} = \frac{T^\chi}{p} \quad (3.1.35)$$

3.2 Discretization of model Boltzmann Equation

3.2.1 Spatial Discretization Using The $a - \varepsilon - \alpha - \beta$ Scheme

In this section, we consider a dimensionless form on the 1D Model Boltzmann equation.

$$\frac{\partial f}{\partial t} + \nu \cdot \frac{\partial f}{\partial x} = C(f) \quad C(f) \rightarrow 0 \quad (3.2.1)$$

Let

$$f^*(x_j, t^n; j, n) = f_j^n, \quad \frac{\partial f^*(x, t; j, n)}{\partial x} = (f_x)_j^n, \quad \frac{\partial f^*(x, t; j, n)}{\partial t} = (f_t)_j^n \quad (3.2.2)$$

Basic on Section 2.1, we can obtain

$$f_j^{n+1} = \frac{1}{2} \left\{ \left(1 - \nu \frac{\Delta t}{\Delta x}\right) \left[f - \left(1 + \nu \frac{\Delta t}{\Delta x}\right) u_x \right]_{j+1}^n + \left(1 + \nu \frac{\Delta t}{\Delta x}\right) \left[f + \left(1 - \nu \frac{\Delta t}{\Delta x}\right) f_x \right]_{j-1}^n \right\} \quad (3.2.3)$$

The above scheme is not equipped to suppress numerical wiggles. We shall describe a remedy for this deficiency.

Let

$$(f_{x^\pm}^{c+})_j^n \stackrel{def}{=} \pm \frac{1}{2} (f_{j\pm 1/2}^n - f_j^n) \quad (3.2.4)$$

Then it can be shown that

$$(f_x^{c+})_j^n = \frac{1}{2} \left[(f_{x^+}^{c+})_j^n + (f_{x^-}^{c+})_j^n \right] \quad (3.2.5)$$

and by eq.(2.3.36), we can obtain

$$W_0 \left((x_-)_j^n, (x_+)_j^n; \alpha \right) = \frac{|x_+|^\alpha x_- + |x_-|^\alpha x_+}{|x_+|^\alpha + |x_-|^\alpha} \quad (|x_+| + |x_-| > 0) \quad (3.2.6)$$

Furthermore, let

$$(f_x^{w+})_j^n \stackrel{def}{=} W_0 \left((f_{x^+}^{c+})_j^n, (f_{x^-}^{c+})_j^n; \alpha \right) \quad (3.2.7)$$

We can be define the $a - \varepsilon - \alpha - \beta$ scheme

$$(f_x^+)_j^n = (f_x^{a+})_j^n + 2\varepsilon (f_x^{c+} - f_x^{a+})_j^n + \beta (f_x^{w+} - f_x^{c+})_j^n \quad (3.2.8)$$

3.2.2 Velocity Discretization Using Discrete Ordinate Method

The distribution function is a function of 3 independent variables. In order to remove the functional dependency on the velocity space of the equations, the discrete ordinate method is applied. This method, which consists of replacing the integration over velocity space of the distribution functions by an appropriate quadrature, requires the values of the distribution function only at certain discrete velocity, that is

$$f(x, v_l, t) = f_l(x, t) \quad (3.2.9)$$

The choice of the discrete values of velocity point is dictated by the considerations that our final interest is not in the distribution functions themselves but in the moments. Hence, the macroscopic moments given by integrals over molecular velocity space can be evaluated by the same quadrature. The discrete ordinate method is then applied to the model Boltzmann equation for the (v_x) velocity space and the resulting differential equations are

$$\frac{\partial f_l}{\partial t} + \frac{\partial v_l f_l}{\partial x} = v(f_l^+ - f_l) \quad (3.2.10)$$

for general coordinate. $l = -N_1, \dots, -1, 1, \dots, N_1$,

Once the discrete distribution function f_l are solved, one can obtain all the moment integrals using Gauss-Hermite quadrature for example as

$$n = \int_{-\infty}^{\infty} f dv_x = \sum_{l=-N_1}^{N_1} W_l f_l e^{v_l^2} \quad (3.2.11)$$

$$nu_x = \int_{-\infty}^{\infty} v_x f dv_x = \sum_{l=-N_1}^{N_1} W_l v_l f_l e^{v_l^2} \quad (3.2.12)$$

$$\frac{3}{2}nT = \int_{-\infty}^{\infty} c^2 f dv_x = \sum_{l=-N_1}^{N_1} W_l v_l^2 f_l e^{v_l^2} - nu_x^2 \quad (3.2.13)$$

$$\tau_{xx} = \int_{-\infty}^{\infty} c_x f dv_x - \frac{1}{2}p = \sum_{l=-N_1}^{N_1} W_l v_l^2 f_l e^{v_l^2} - nu_x^2 - \frac{1}{2}p \quad (3.2.14)$$

$$q_x = \int_{-\infty}^{\infty} c_x c^2 f dv_x = \int_{-\infty}^{\infty} v_x v_x^2 f dv_x - 2u_x \int_{-\infty}^{\infty} v_x^2 f dv_x - nu_x u_x^2 - \frac{3}{2}nu_x T \quad (3.2.15)$$

3.2.3 Treatment of Source Terms

We will Model Boltzmann equation

$$\frac{\partial f}{\partial t} + \frac{\partial f}{\partial x} = \nu_c (f_M - f) \quad (3.2.16)$$

Refer to the reference paper [2], the source term would be calculated at $n+1/2$ time level,

$$f_j^{n+1/2} = \frac{1}{2} \left\{ \left(1 - \nu \frac{\Delta t}{\Delta x}\right) \left[f - \left(1 + \nu \frac{\Delta t}{\Delta x}\right) f_{\bar{x}} \right]_j^n + \left(1 + \nu \frac{\Delta t}{\Delta x}\right) \left[f + \left(1 - \nu \frac{\Delta t}{\Delta x}\right) f_{\bar{x}} \right]_{j-1}^n \right\} + [\nu (f_M - f)]_j^{n+1/2} \quad (3.2.17)$$

Since ν and f_M are nonlinearly dependent with f , the above nonlinearly equation can be solved by Newton-Raphson method or secant method.

The above equation also can be simplified to the form

$$f_j^{n+1/2} = \frac{1}{2} \left\{ \left(1 - \nu \frac{\Delta t}{\Delta x}\right) \left[f - \left(1 + \nu \frac{\Delta t}{\Delta x}\right) f_{\bar{x}} \right]_j^n + \left(1 + \nu \frac{\Delta t}{\Delta x}\right) \left[f + \left(1 - \nu \frac{\Delta t}{\Delta x}\right) f_{\bar{x}} \right]_{j-1}^n \right\} + \left[\nu^* (f_M^* - f) \right]_j^{n+1/2}$$

(3.2.18)

Where ν^* and f_M^* are calculated with f^* which is obtained from

$$f_j^* = \frac{1}{2} \left\{ \left(1 - \nu \frac{\Delta t}{\Delta x}\right) \left[f - \left(1 + \nu \frac{\Delta t}{\Delta x}\right) f_{\bar{x}} \right]_j^n + \left(1 + \nu \frac{\Delta t}{\Delta x}\right) \left[f + \left(1 - \nu \frac{\Delta t}{\Delta x}\right) f_{\bar{x}} \right]_{j-1}^n \right\}$$

(3.2.19)



Chapter 4 Results and Discussions

4.1 Overview

Five shock problems are selected to test the MBE solver and Euler equation. In all cases the ratio of specific heat is $\gamma=1.667$. The numerical results are calculated on a mesh $N=100$ points, and simulation region form -1 to 1 . Table 1 shows all test case initial conditions. In addition, we simulation test 1 with different kundsen number 1, 0.1, 0.01, 0.001, and 1E-5. Fig. 2~Fig.6, show exact solution profiles.

4.2 Results of the Euler Equation Using the CESE Model

In numerical results, solid line is exact solution, rhomb is Euler equation for CESE method, and right triangle is Euler equation for MBE method. Exact solution is by E. F. Toro "Riemann Solvers and Numerical Methods for Fluid Dynamics", 1997. In test 1 (See Fig.7~Fig.11), is simple shock tube problem. This is a very mild test and its solution consists of a left rarefaction, a contact and a right shock. The numerical result, Euler equation for CESE method, and Euler equation for MBE method are all similarity exact solution. In test 2(See Fig.12~Fig.15), the solution contains a left rarefaction, a contact and a right shock. In test 3 (See Fig.16~Fig.19.), its solution contains a left shock, a contact discontinuity and a right rarefaction. In front of two test case, velocity and pressure will be near the end of a constant, of course, get the

simulation results are also very close exact solution, In test 4 (See Fig20~Fig.23), has solution consisting two strong rarefactions and a trivial stationary contact discontinuity. MBE method in the numerical simulation results, in the temperature, the answer has not been nearly exact solution. Because the initial conditions of low temperature, resulting in insufficient velocity distribution, so integral, the answer to be inaccurate, Makes the simulation time is not accurate. In Test 5(See Fig.24~Fig.27), its solution represents the collision of the these two strong shocks and consists of a left facing shock, a right traveling contact discontinuity and a right traveling shock wave. The simulation results are very close to exact solution.

4.3 Results of the Model Boltzmann Using the CESE Model

We simulation difference Knudsen number in test 1, respective $kn=1,0.1,0.01,0.001$, and $kn \rightarrow 0$. From the simulation results can know that when Knudsen number more small, the phenomenon of the more obvious shock wave. By Fig.28~Fig.31 know, Knudsen number = 0.001, $1 \text{ E-}5$, and $1 \text{ E-}20$, which is almost three overlapping together. Knudsen number = 0.001 on the results have been very close exact solution. Even can be calculated to Knudsen number = $1 \text{ E-}20$, can be good simulation results.

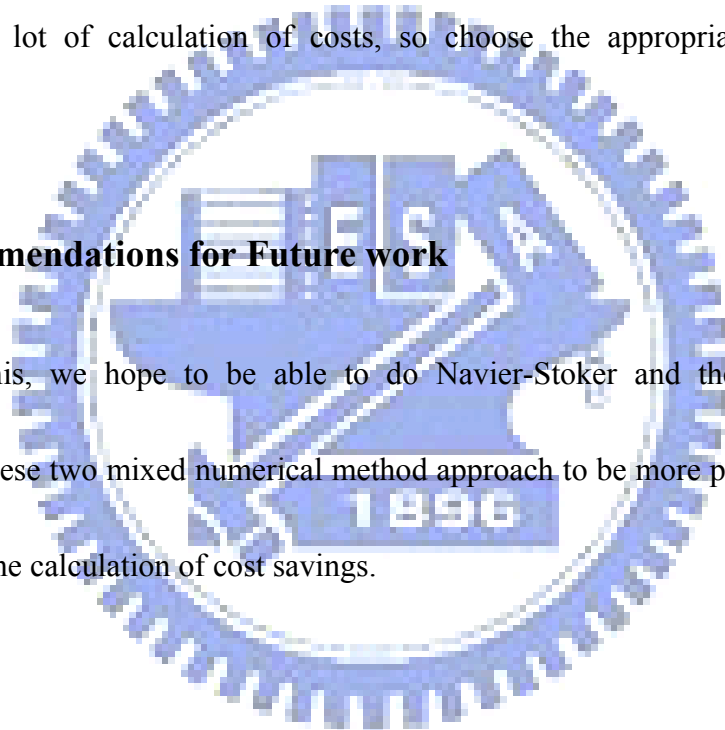
Chapter 5 Conclusion

5.1 Summery

The results are very close to exact solution. But disadvantage is that when the temperature is not large, a representative enough velocity distribution, accurate integral to the outcome of the case, ΔV be changed very little, But to do so results will bring a lot of calculation of costs, so choose the appropriate ΔV is very important.

5.2 Recommendations for Future work

After this, we hope to be able to do Navier-Stoker and the MBE method combining these two mixed numerical method approach to be more precise numerical results, and the calculation of cost savings.



References:

1. Sin-Chung Chang , “The Method of Space-Time Conservation Element and Solution Element –A New Approach for Solving the Navier-Stokes and Euler Equations”, Journal of Computational Physics ,Vol 119, pp. 295-324,1995.
2. Shang-Tao Yu and Sin-Chung Chang, “Treatments of Stiff Source Terms in Conservation Laws by the Method of Space-Time Conservation Element and Solution Element”, AIAA, 1997.
3. Sin-Chung Chang ,e.g, “Robust and simple Non-Reflecting Boundary Conditions for the Euler Equations-A New Approach Based on the Space-Time CE/SE Method”, NASA/TM-2003-212495/REV1, May 2005.
4. Shamsul Qamar and Gerald Warnecke, “A Space-Time Conservative Method for Hyperbolic Systems with Stiff and Non Stiff Source Terms”, Commun. Comput. Phys. , Vol. 1, No. 3, pp. 449-478,2006.
5. S. F. L , V. R, and G. R, “Central Schemes for Balance Laws of Relaxation Type”, SIAM . J. NUMER. ANAL. , Vol. 38, No. 4. pp. 1337-1356
6. E. Gabetta, L. Pareschi, and M. Ronconi, “Central Schemes for hydrodynamical limits of discrete-velocity kinetic models” ,Transport Theory and Statistical Physics, 29(3-5), 465-477(2000)
7. Sin-Chung Chang, Xiao-Yen Wang, and Wai-Ming To, “Application of the Space-Time Conservation Element Method to One-Dimensional Convection –Diffusion Problems”, J. C. Phys. 165, 189-215 (2000)

	L			R					
	D	U	P	D	U	P	α	ε	kn
Teat 1	1	0	1	0.125	0	0.1	2	0.1	0.01
Teat 2	0.445	0	3.526	0.5	0	0.57	2	0.2	0.01
Teat 3	0.445	0	0.57	0.5	0	3.526	2	0.1	0.01
Teat 4	1	-1	0.4	1	1	0.4	2	0.2	0.01
Teat 5	5.9992	19.598	460.89	5.9924	-6.196	46.095	2	0.1	0.01

Table 1 Initial conditions for five test problems.



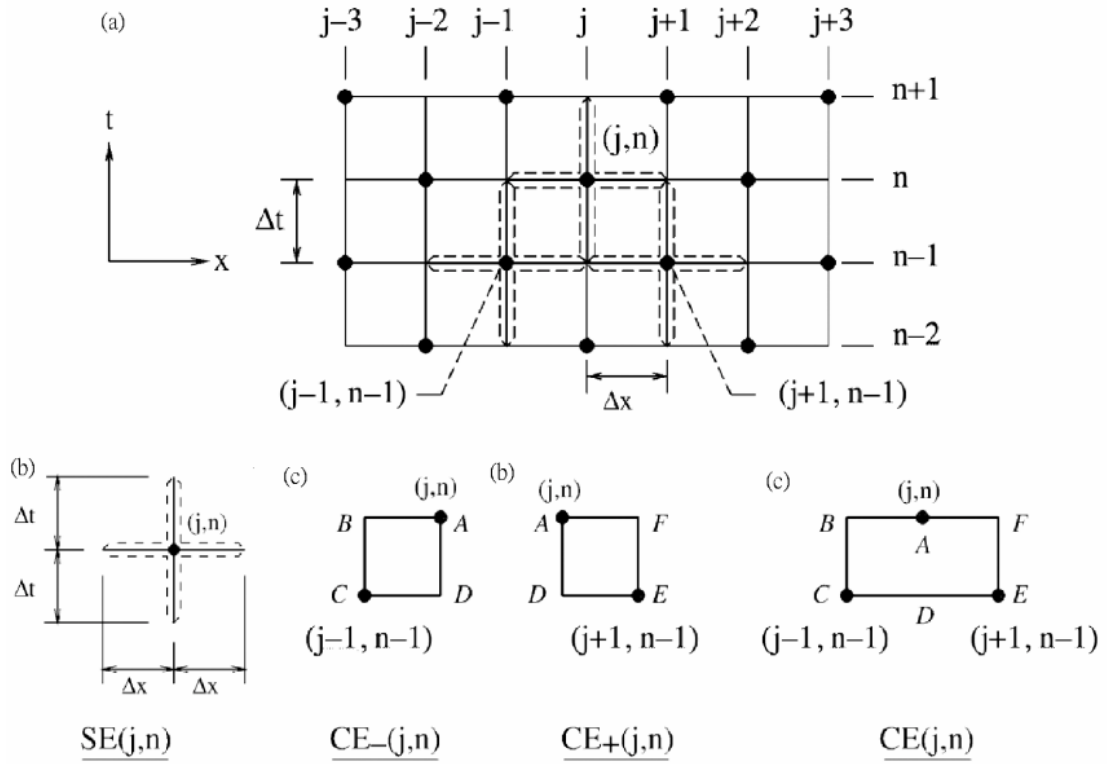
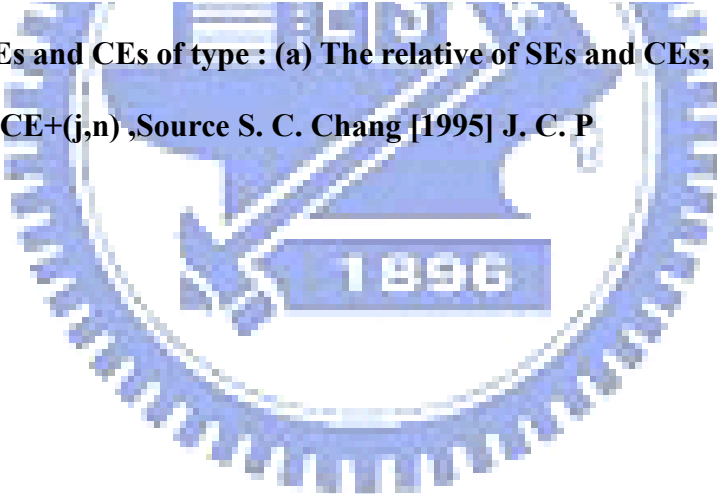


Fig. 1. The SEs and CEs of type : (a) The relative of SEs and CEs; (b) SEs(j,n); (c) CE-(j,n); (d) CE+(j,n), Source S. C. Chang [1995] J. C. P



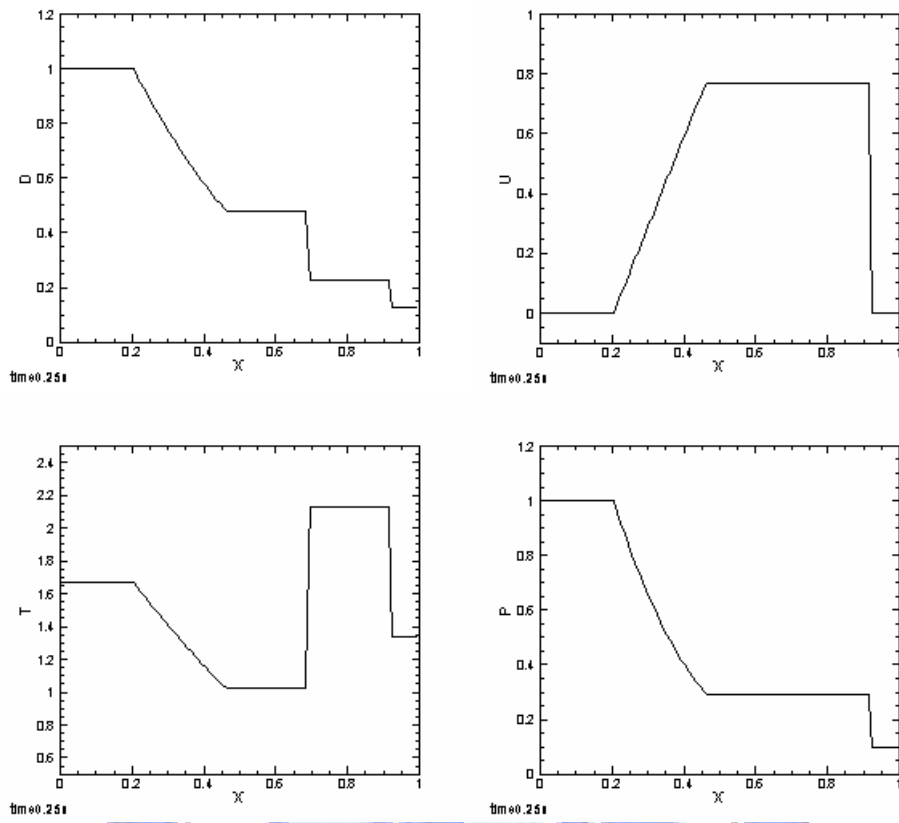
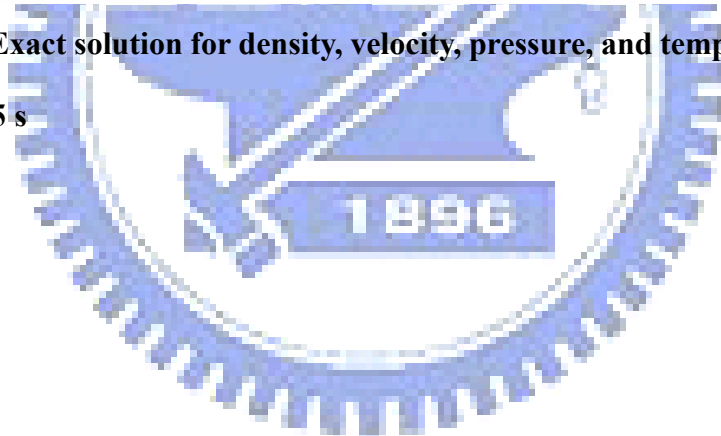


Fig.2 Test 1 Exact solution for density, velocity, pressure, and temperature at time $t = 0.25$ s



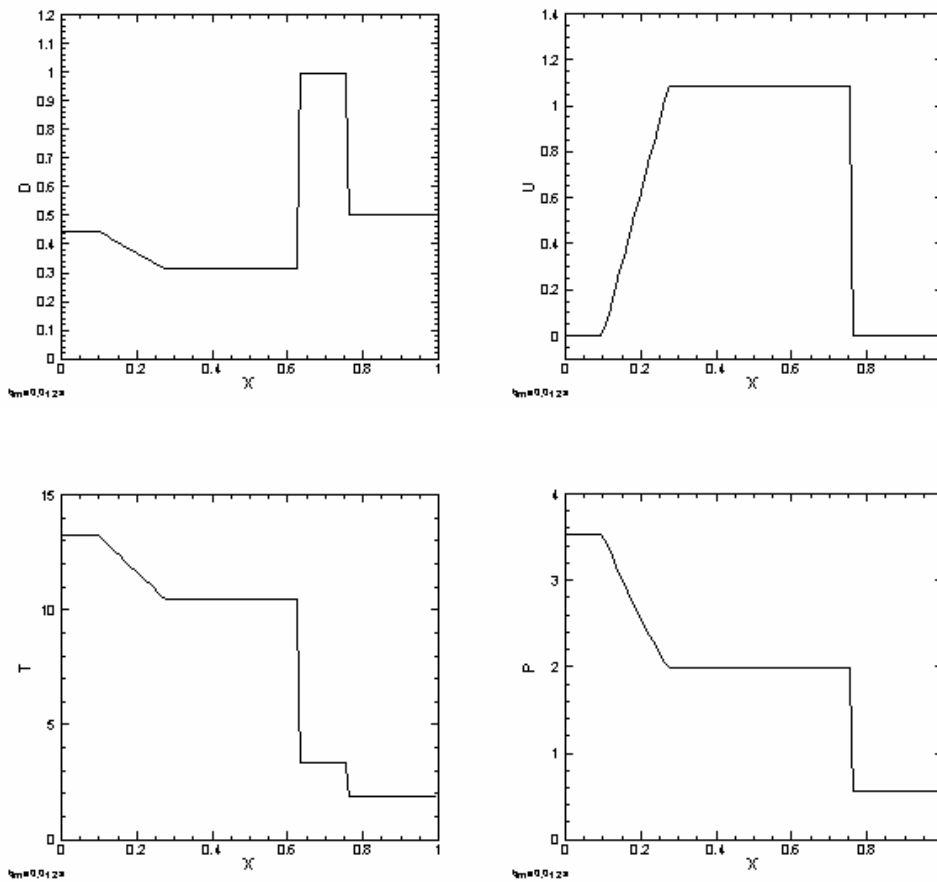
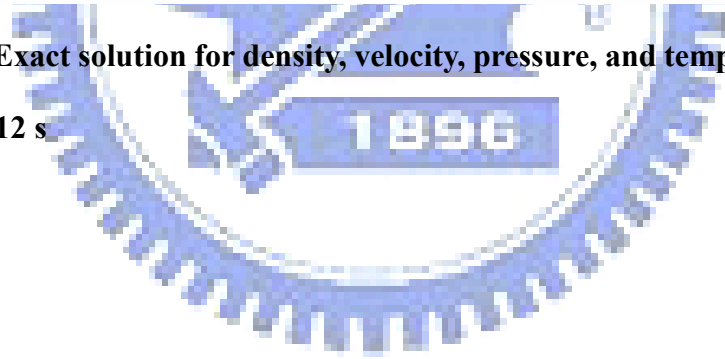


Fig.3 Test 2 Exact solution for density, velocity, pressure, and temperature at time $t = 0.012$ s



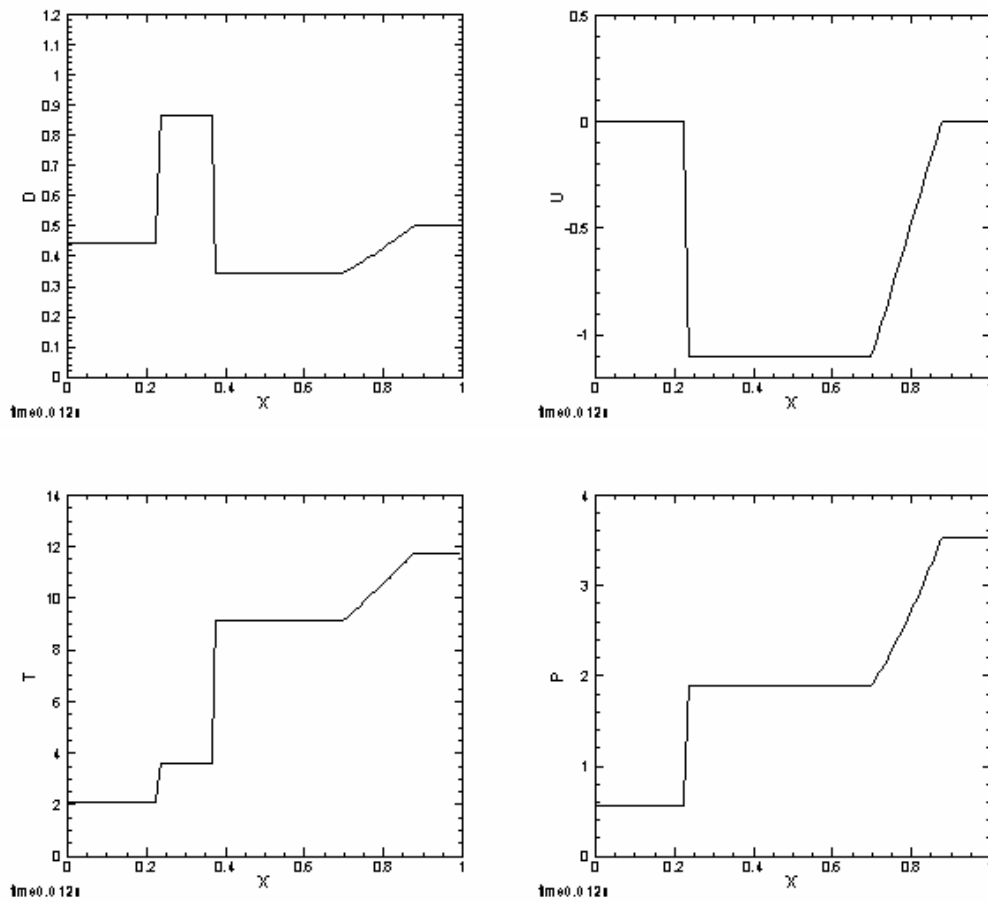


Fig.4 Test 3 Exact solution for density, velocity, pressure, and temperature at time $t = 0.012$ s

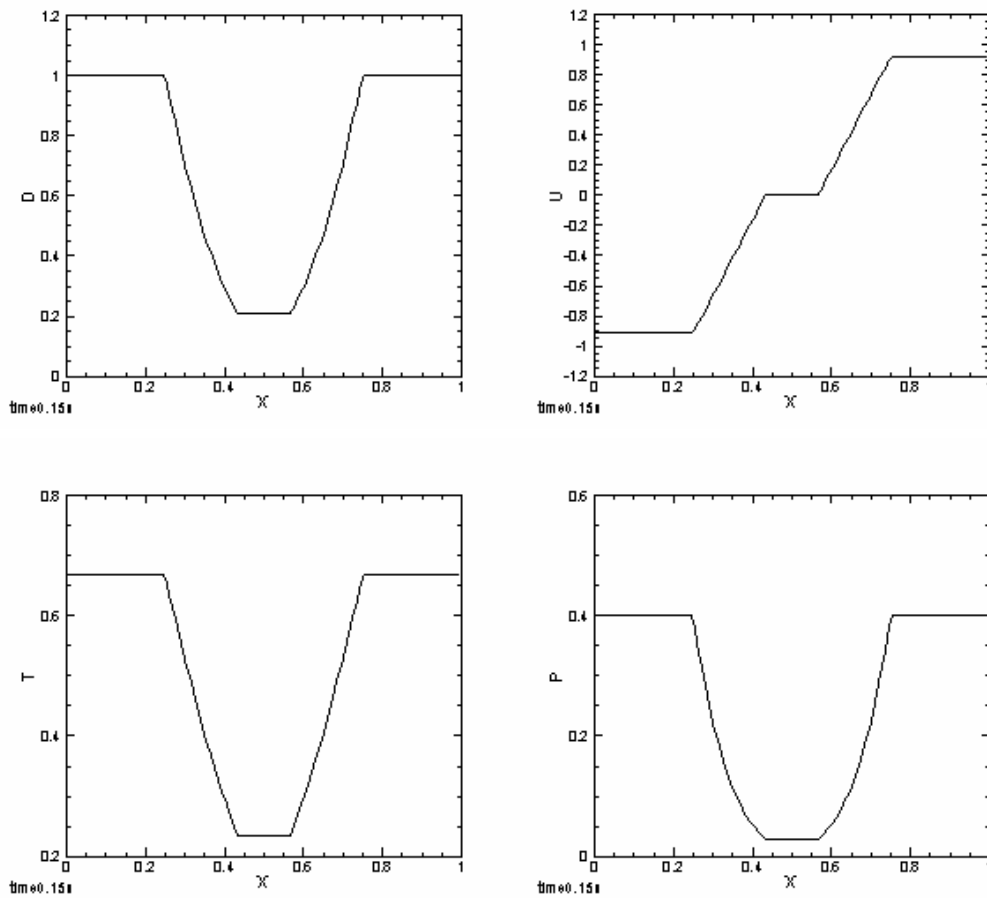


Fig.5 Test 4 Exact solution for density, velocity, pressure, and temperature at time $t = 0.15$ s

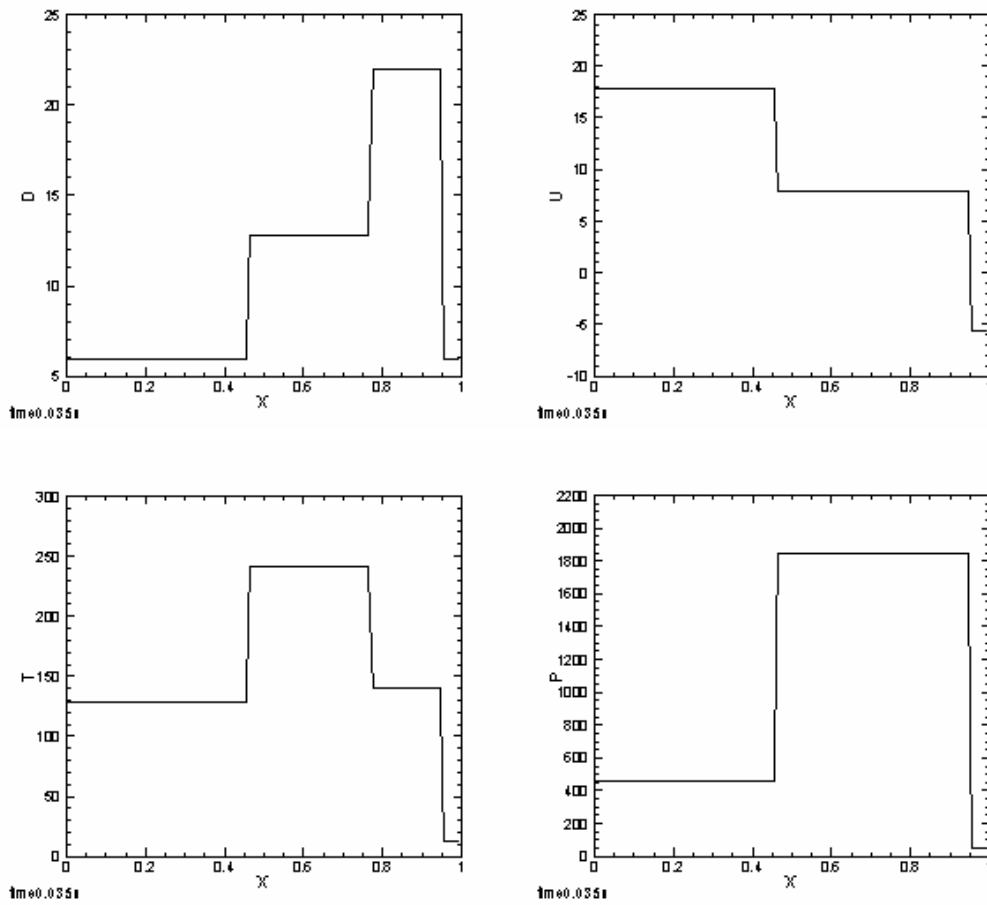


Fig.6 Test 5 Exact solution for density, velocity, pressure, and temperature at time $t = 0.25$ s



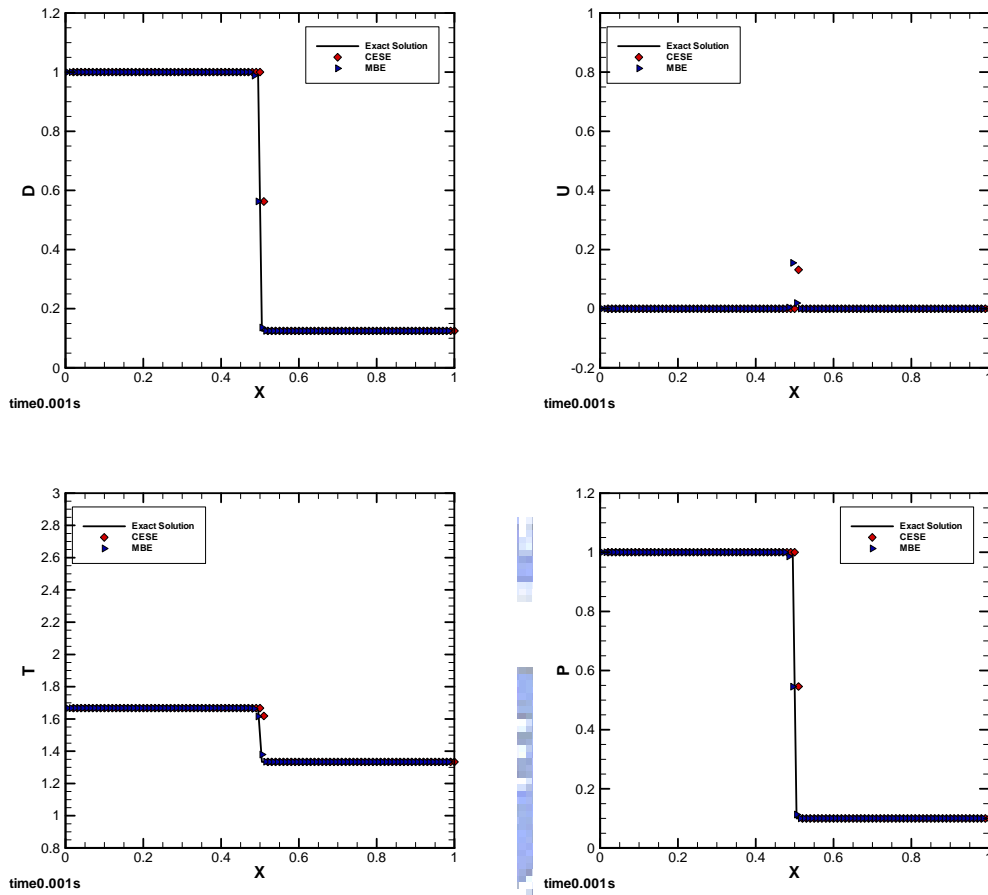
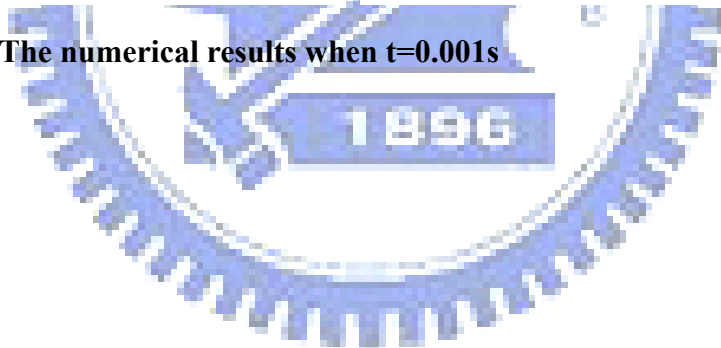


Fig.7 Test 1: The numerical results when $t=0.001s$



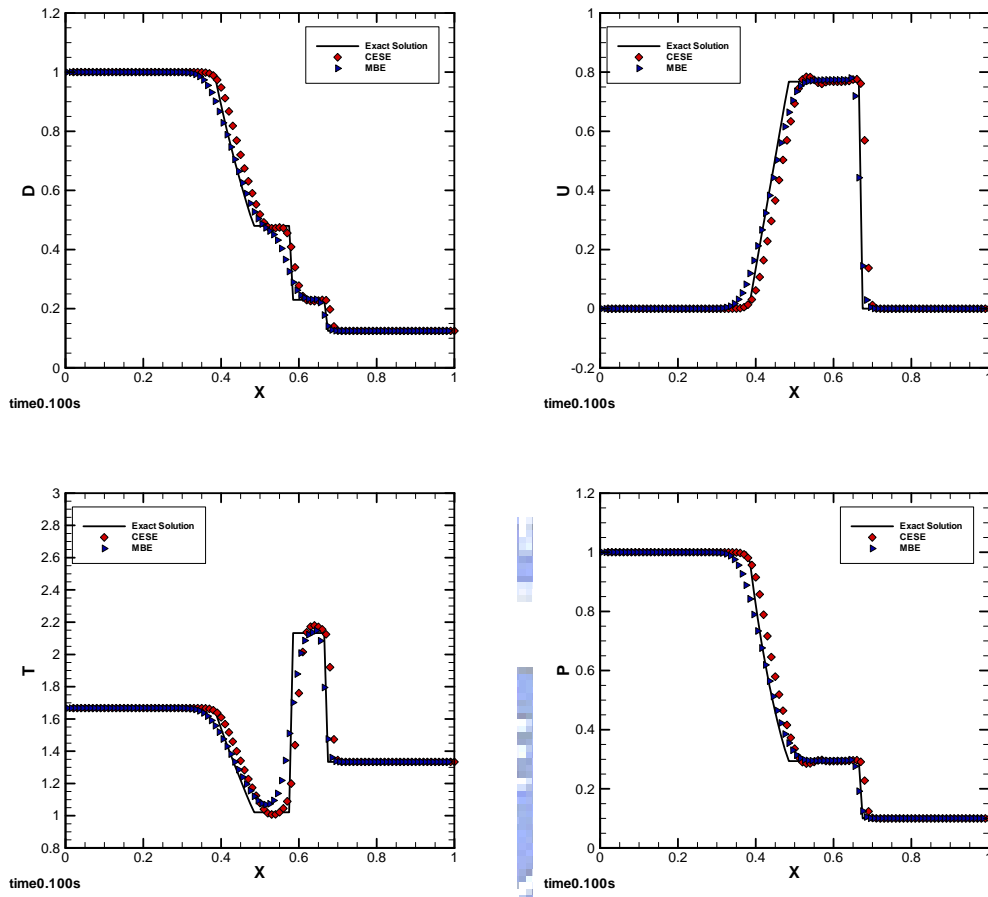
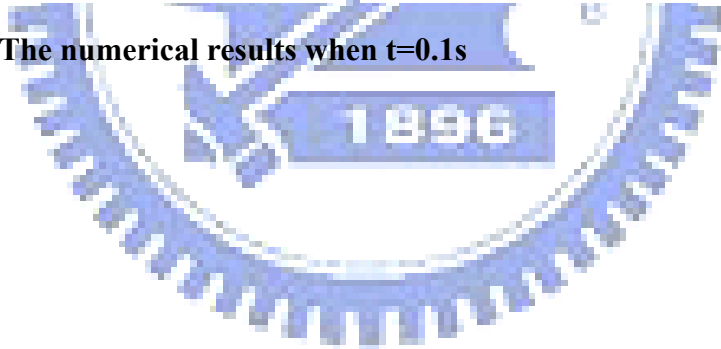


Fig.8 Test 1: The numerical results when $t=0.1$ s



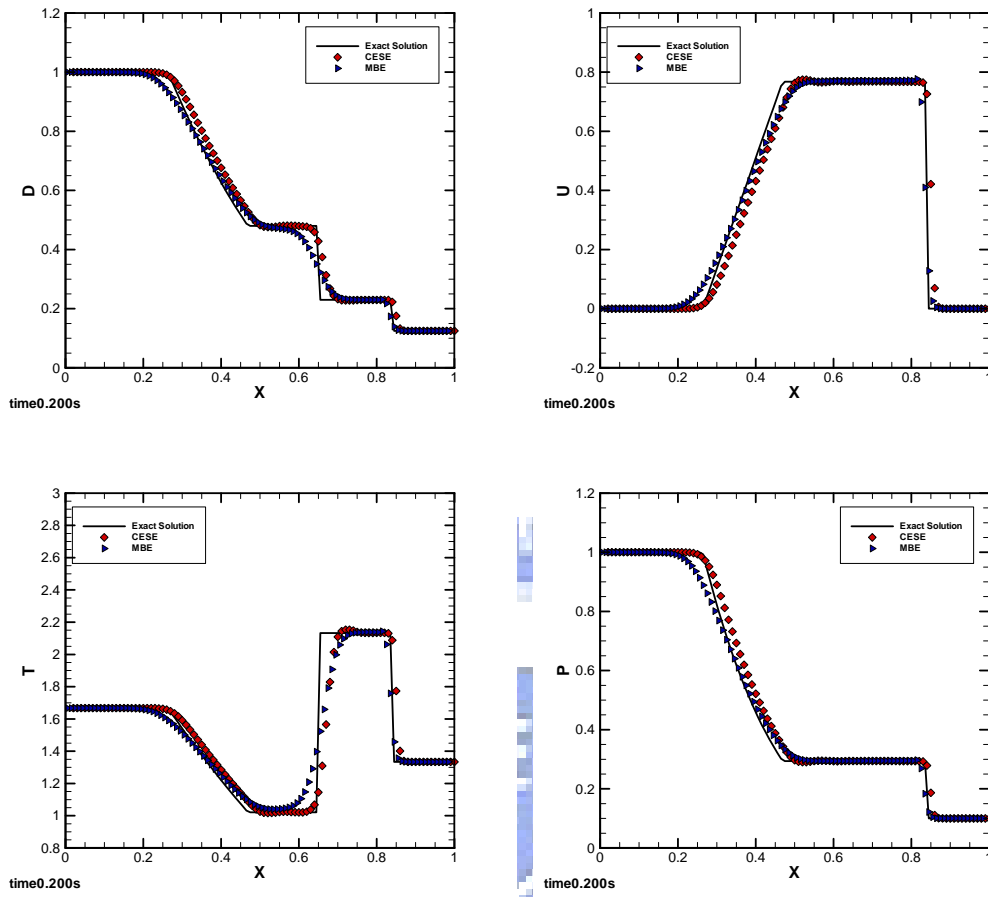
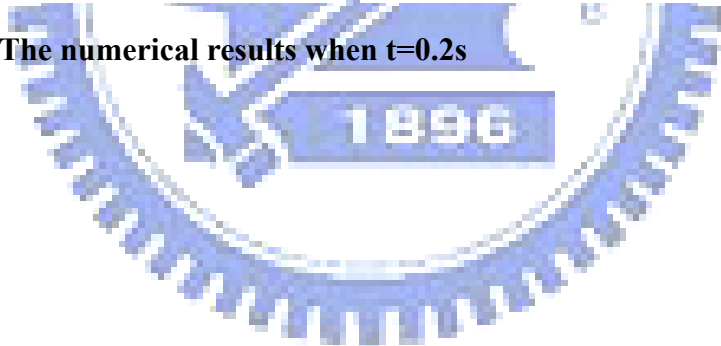


Fig.9 Test 1: The numerical results when $t=0.2$ s



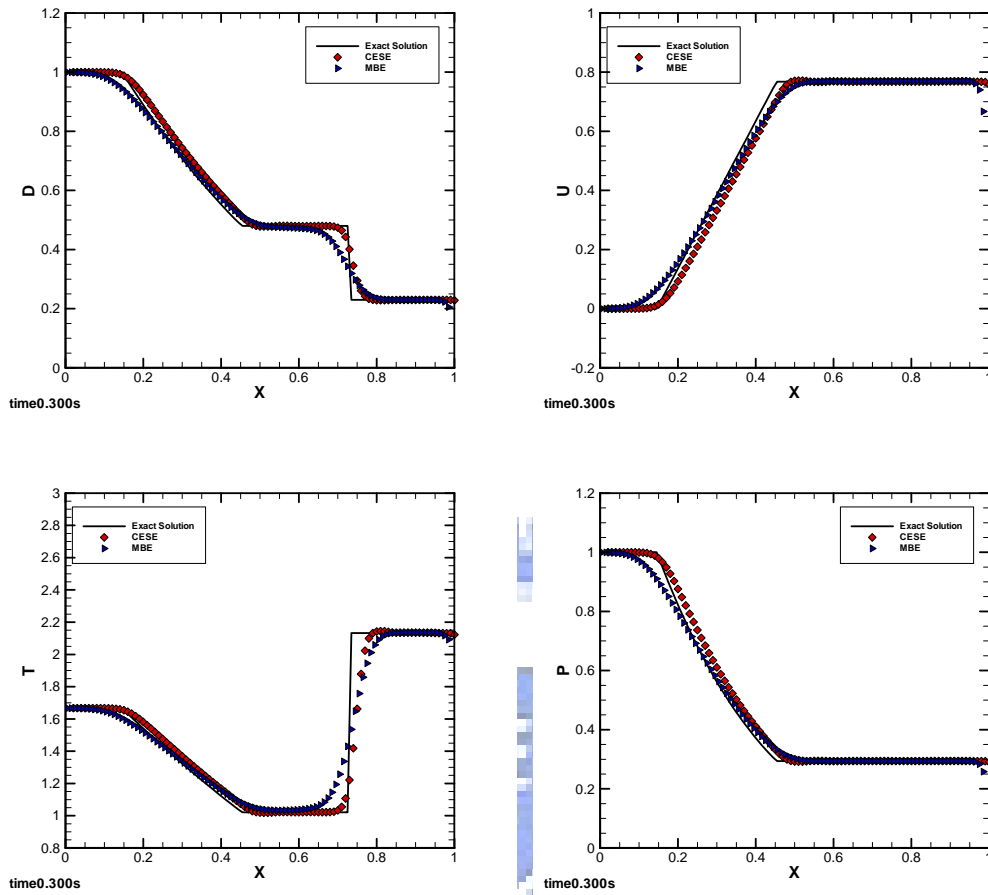
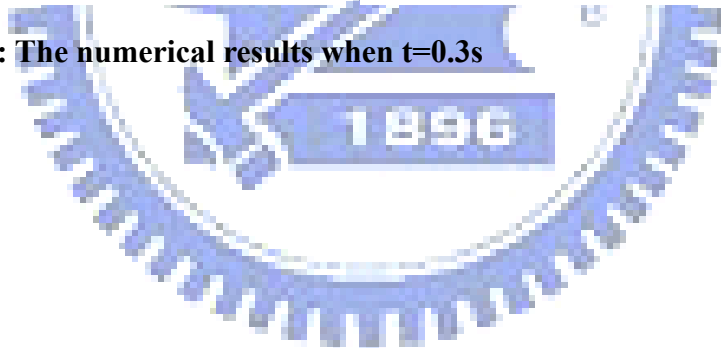


Fig.10 Test 1: The numerical results when $t=0.3s$



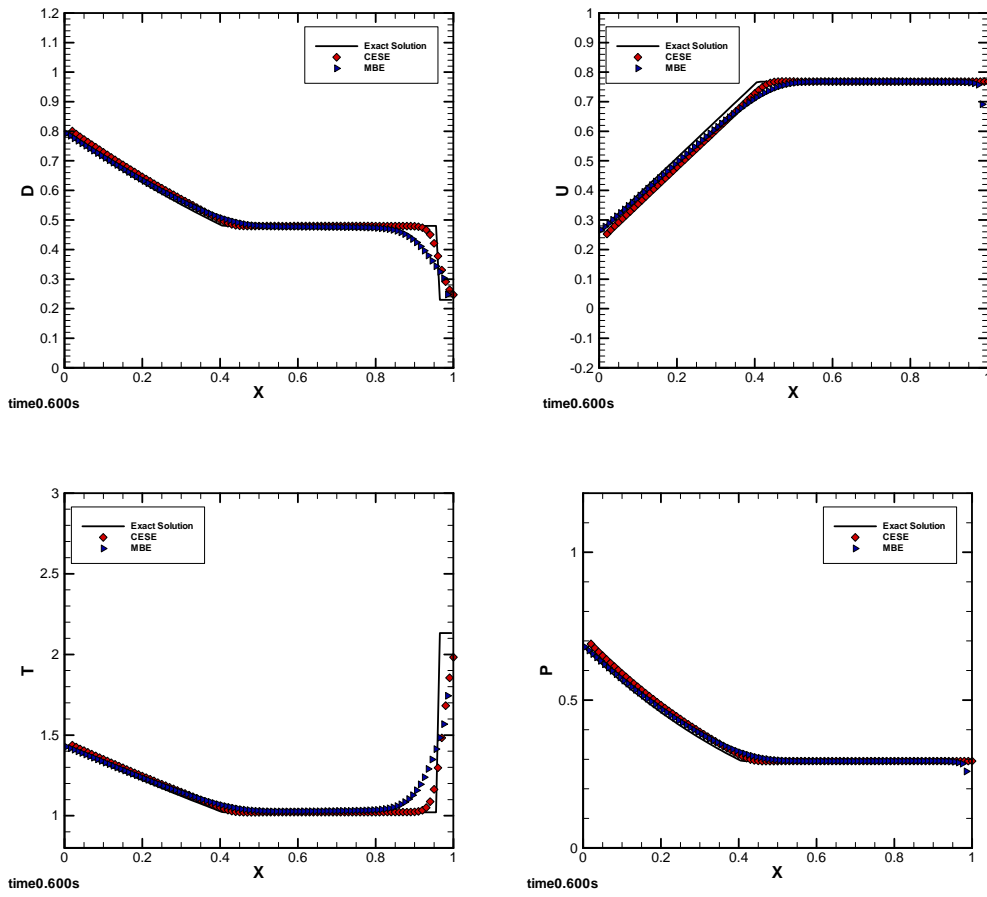
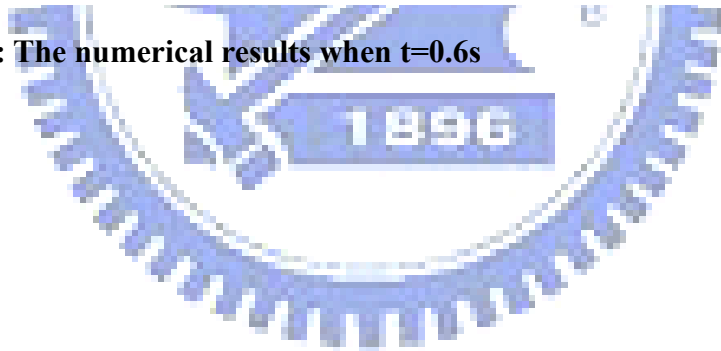


Fig.11 Test 1: The numerical results when $t=0.6s$



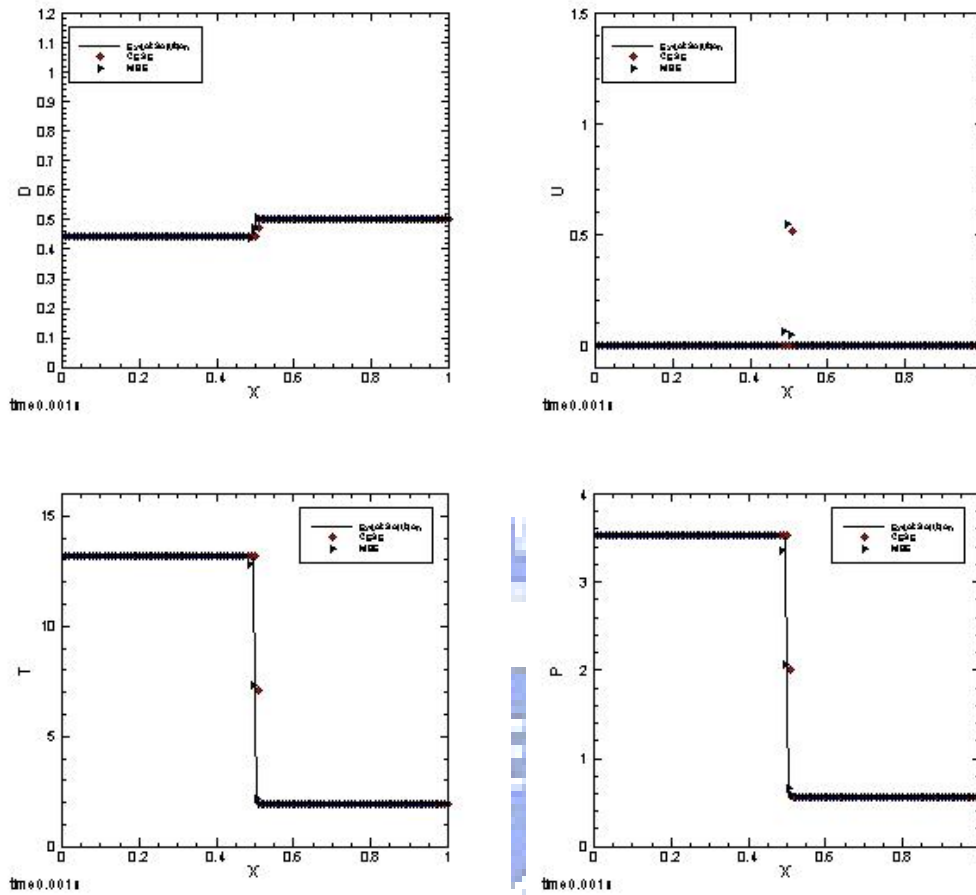


Fig.12 Test 2: The numerical results when $t=0.001s$



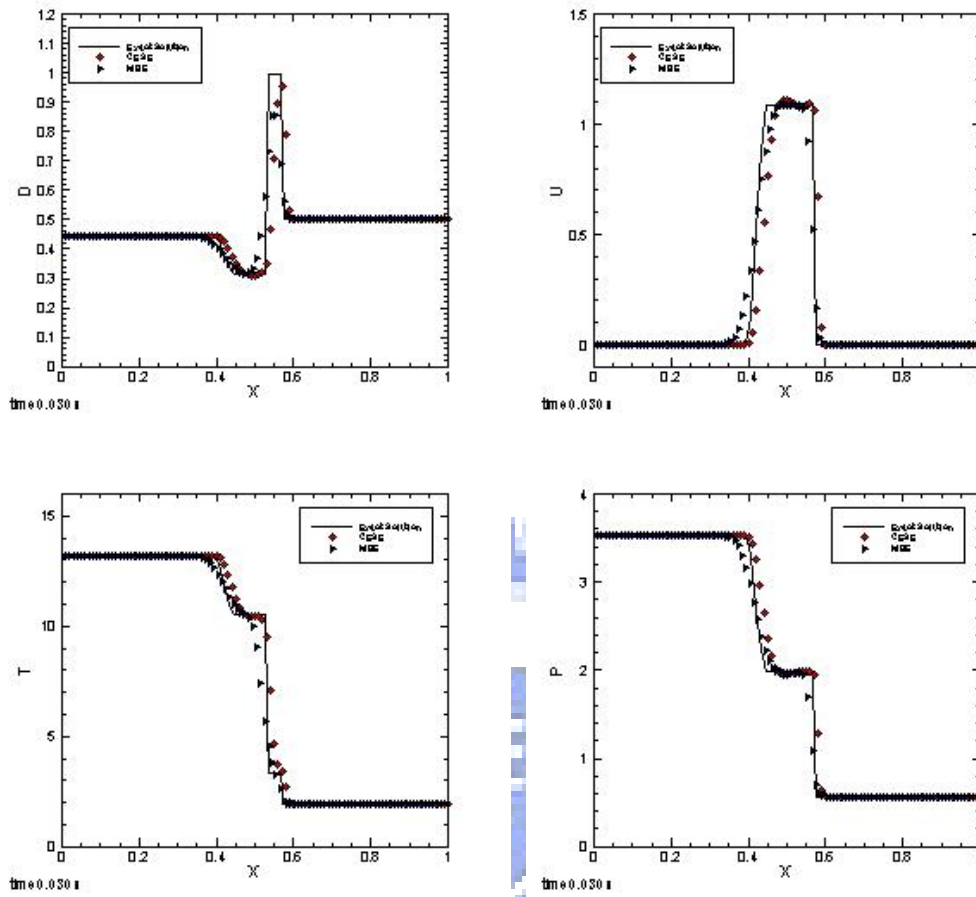
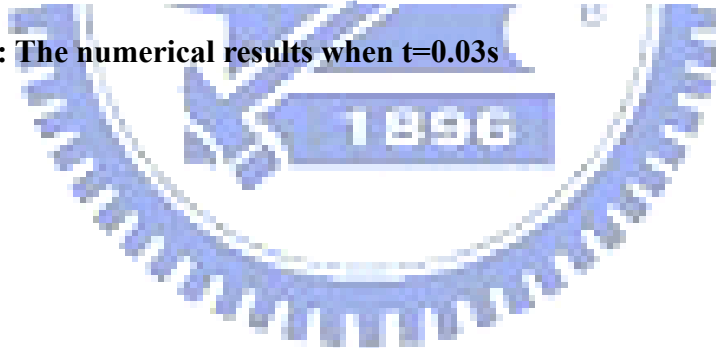


Fig.13 Test 2: The numerical results when $t=0.03$ s



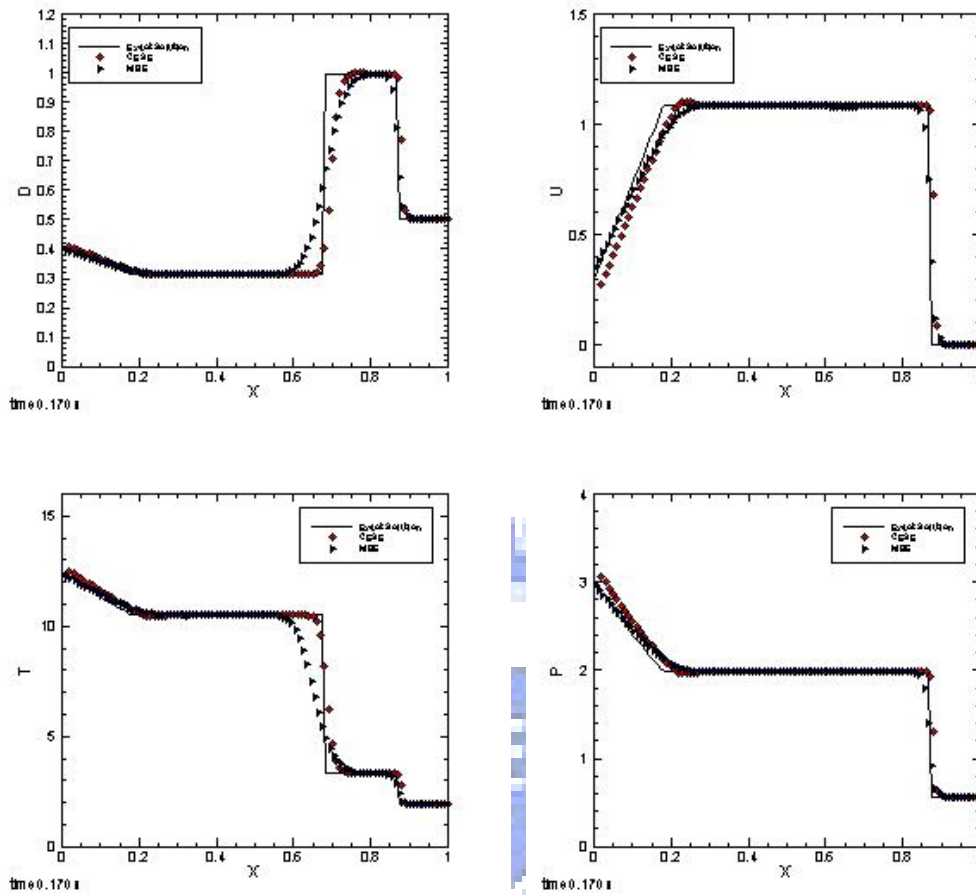


Fig.14 Test 2: The numerical results when $t=0.17$ s



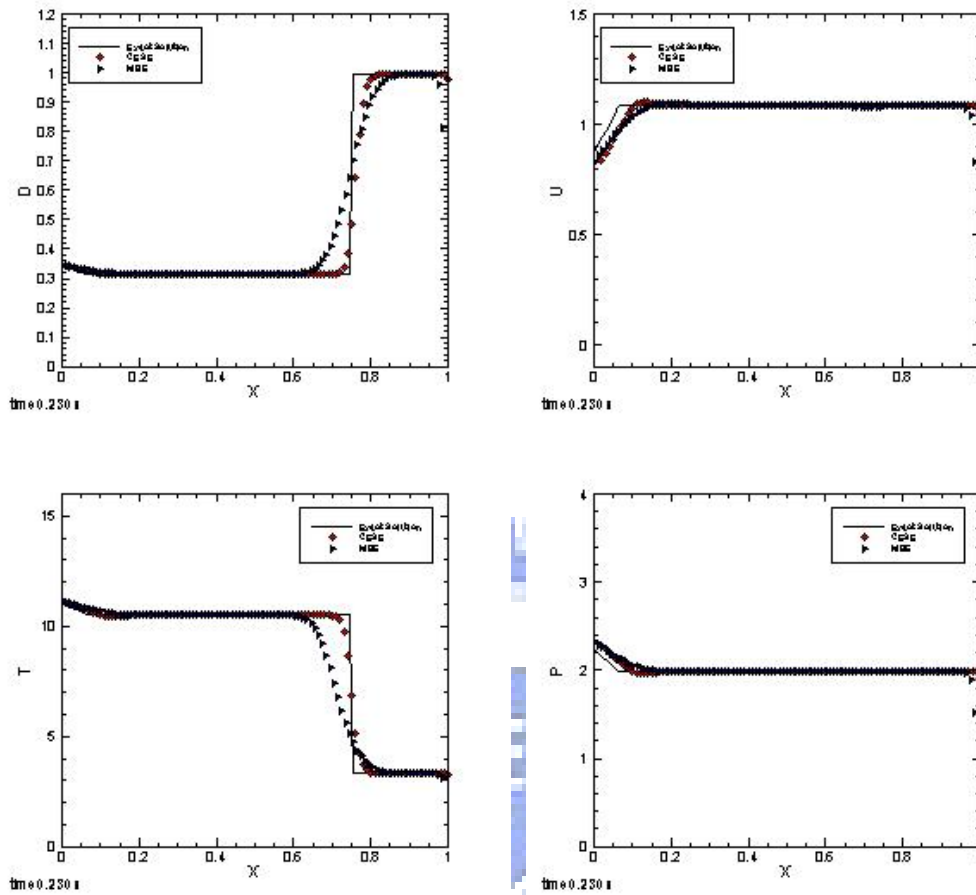


Fig.15 Test 2: The numerical results when $t=0.23$ s



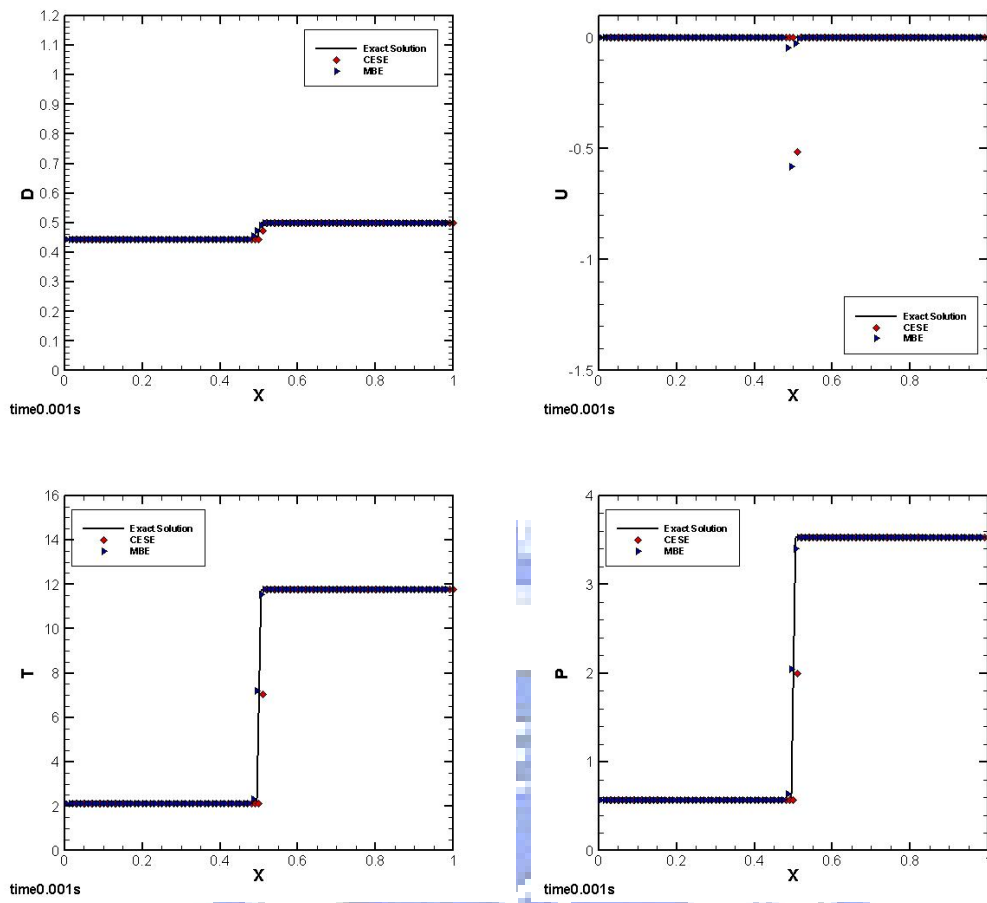
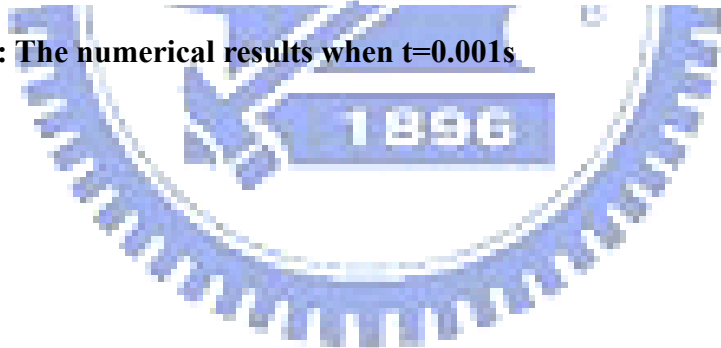


Fig.16 Test 3: The numerical results when $t=0.001s$



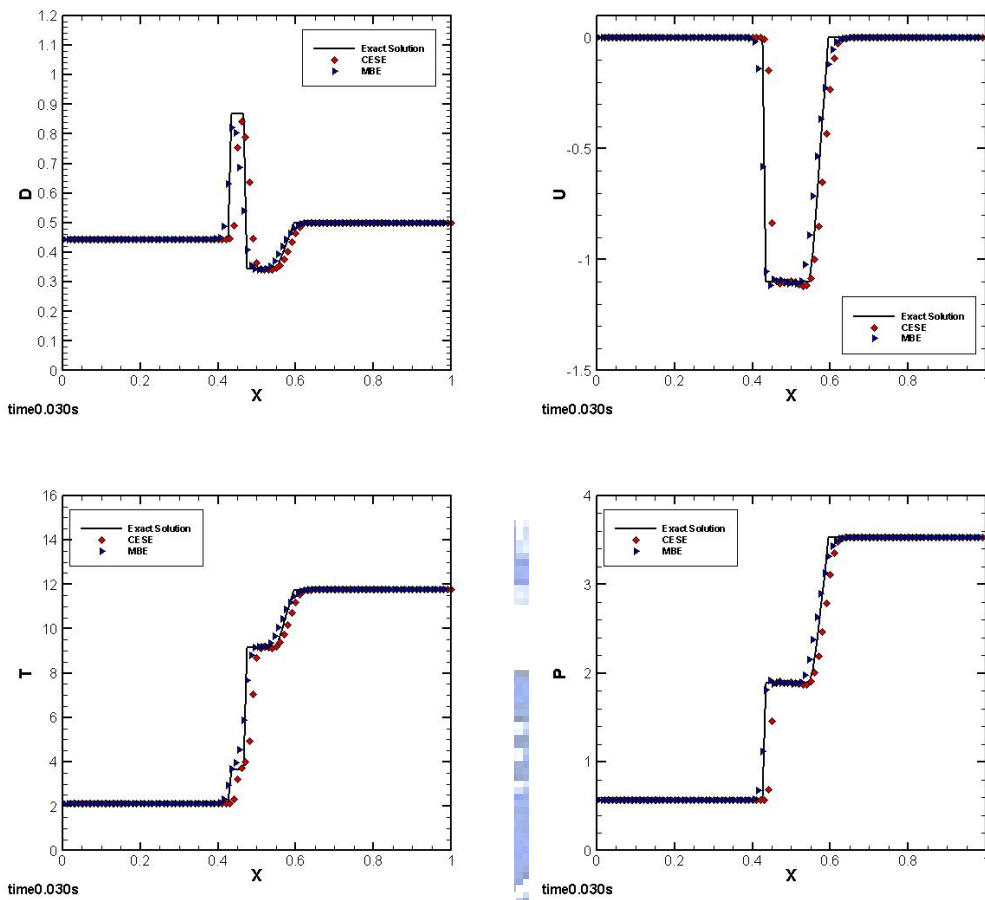
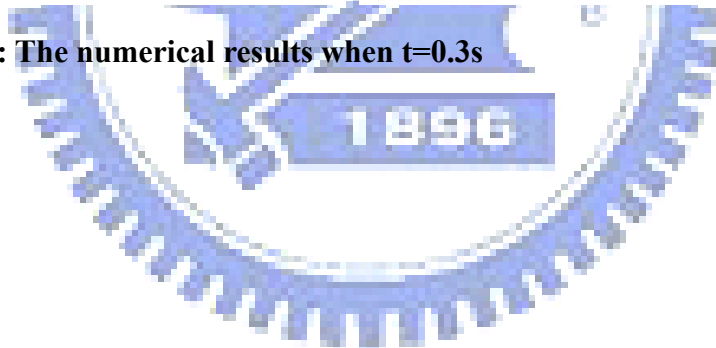


Fig.17 Test 3: The numerical results when $t=0.3s$



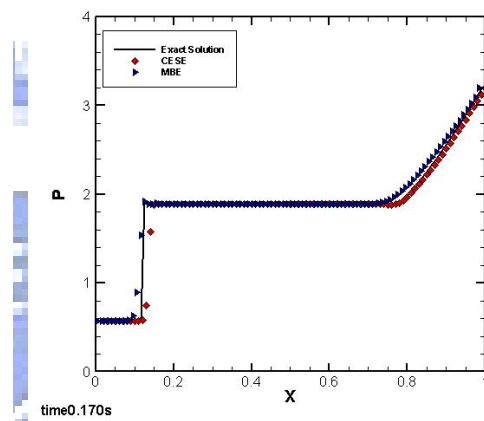
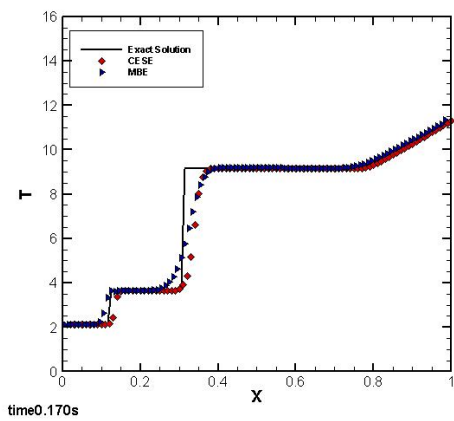
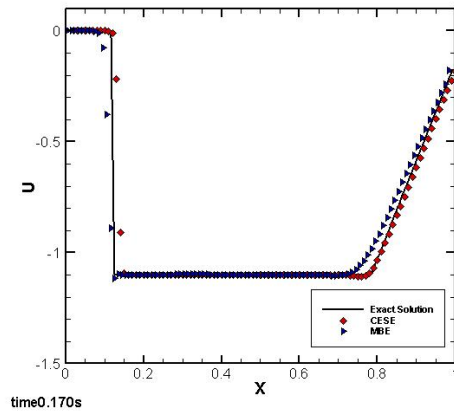
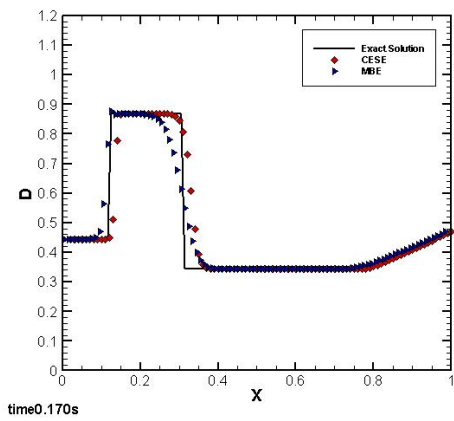
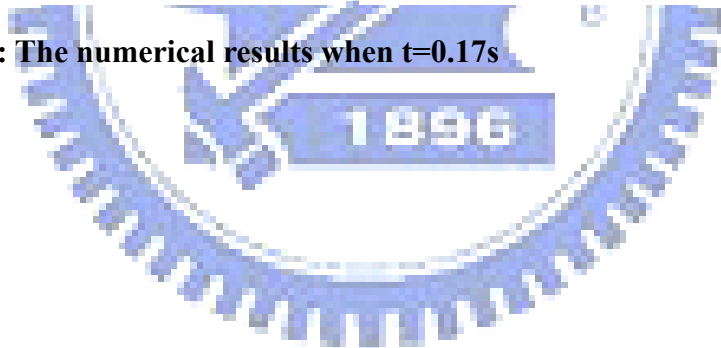


Fig.18 Test 3: The numerical results when $t=0.17s$



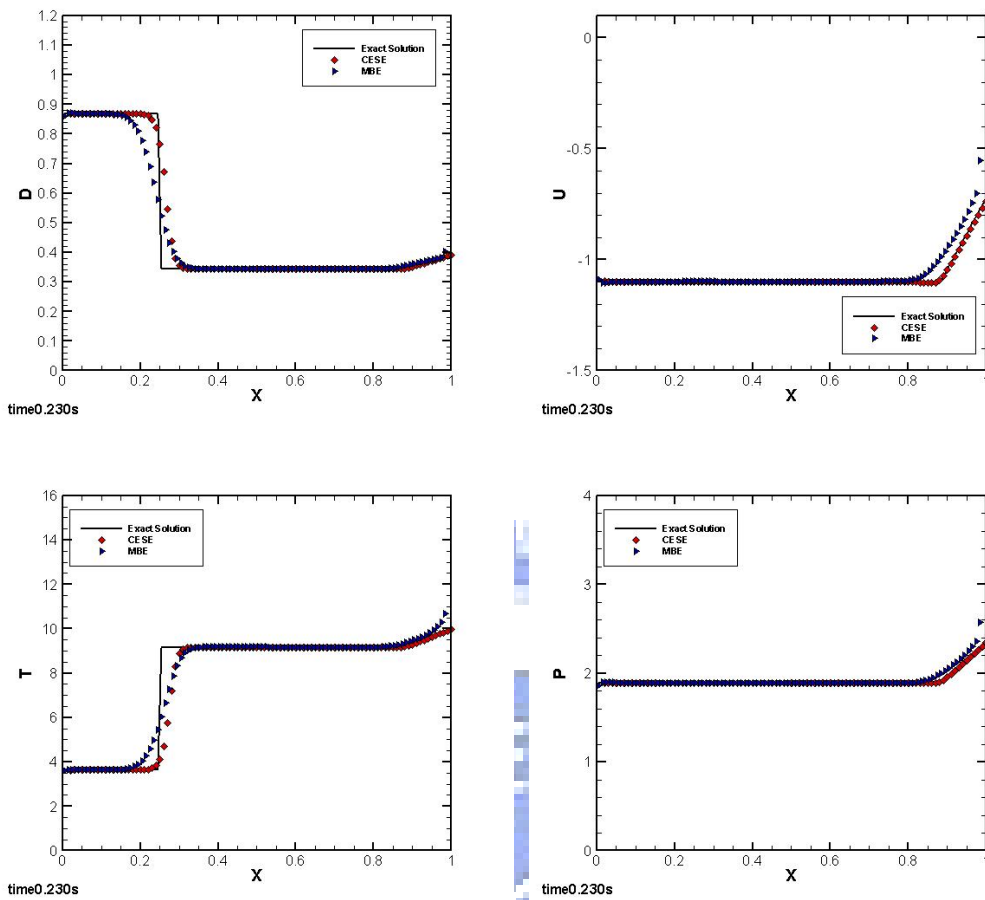
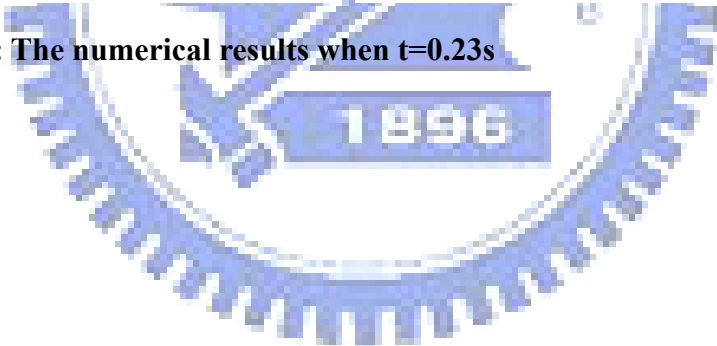


Fig.19 Test 3: The numerical results when t=0.23s



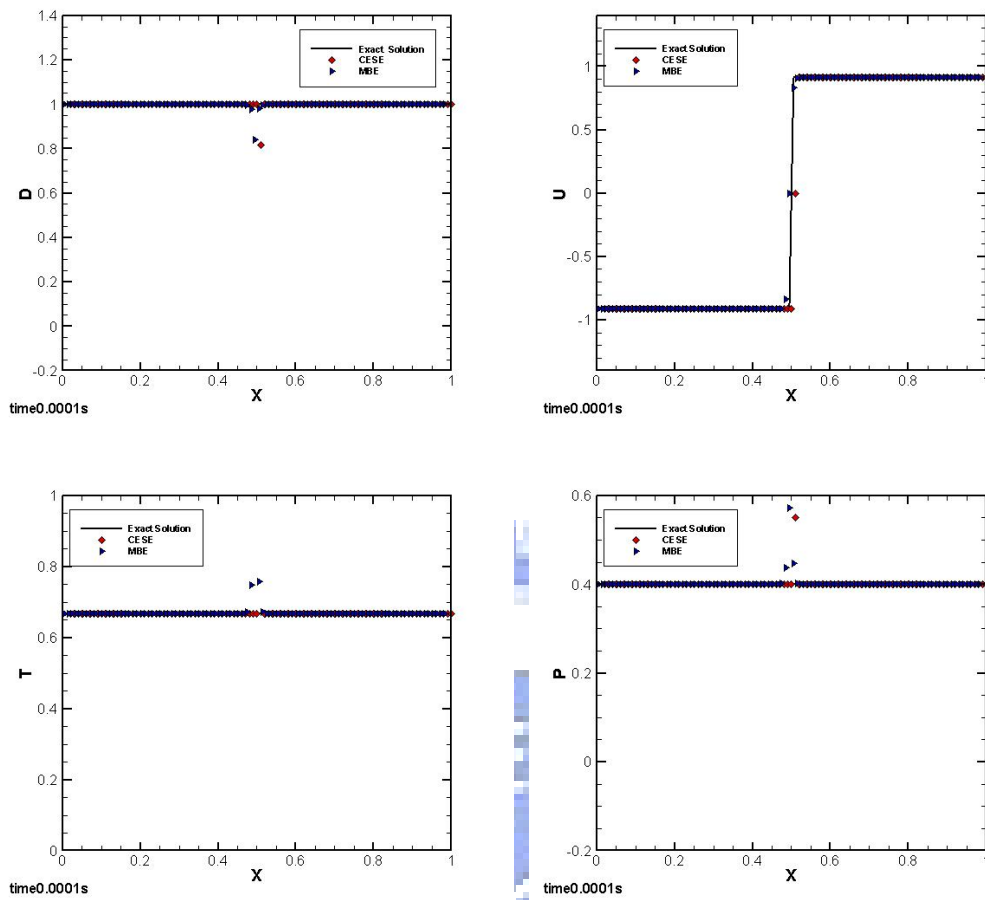


Fig.20 Test 4: The numerical results when $t=0.001s$



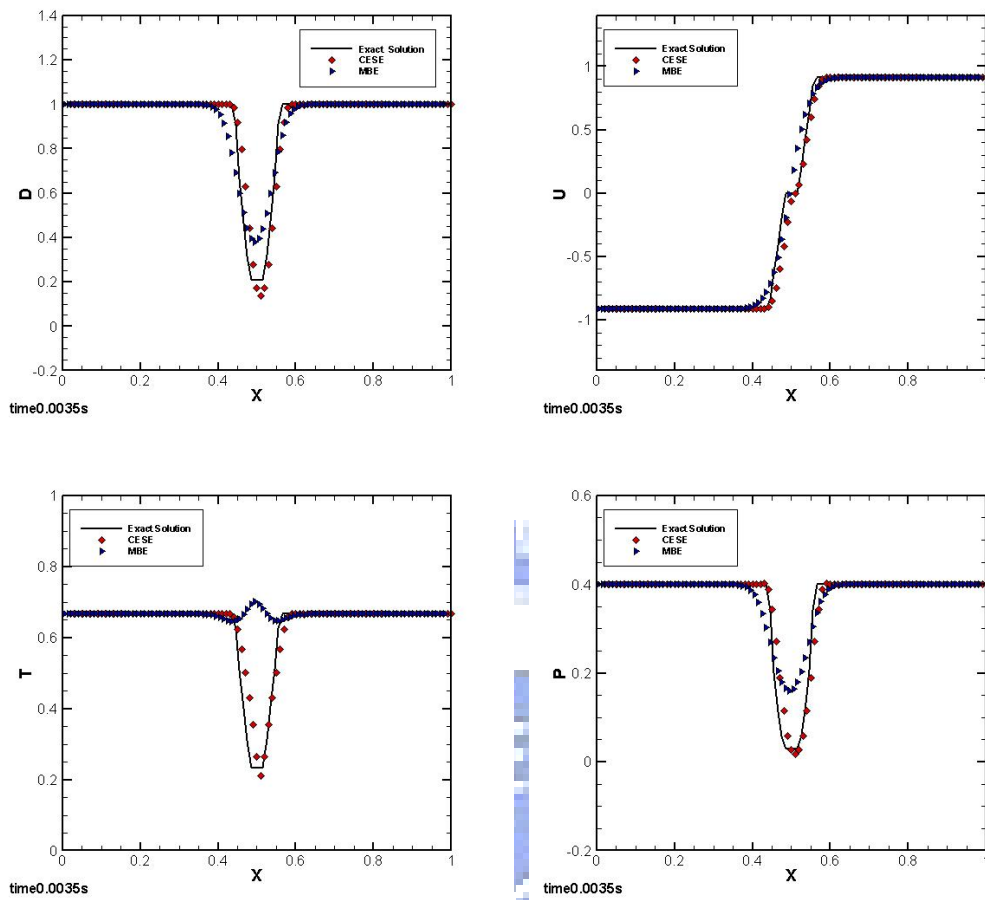


Fig.21 Test 4: The numerical results when $t=0.035s$



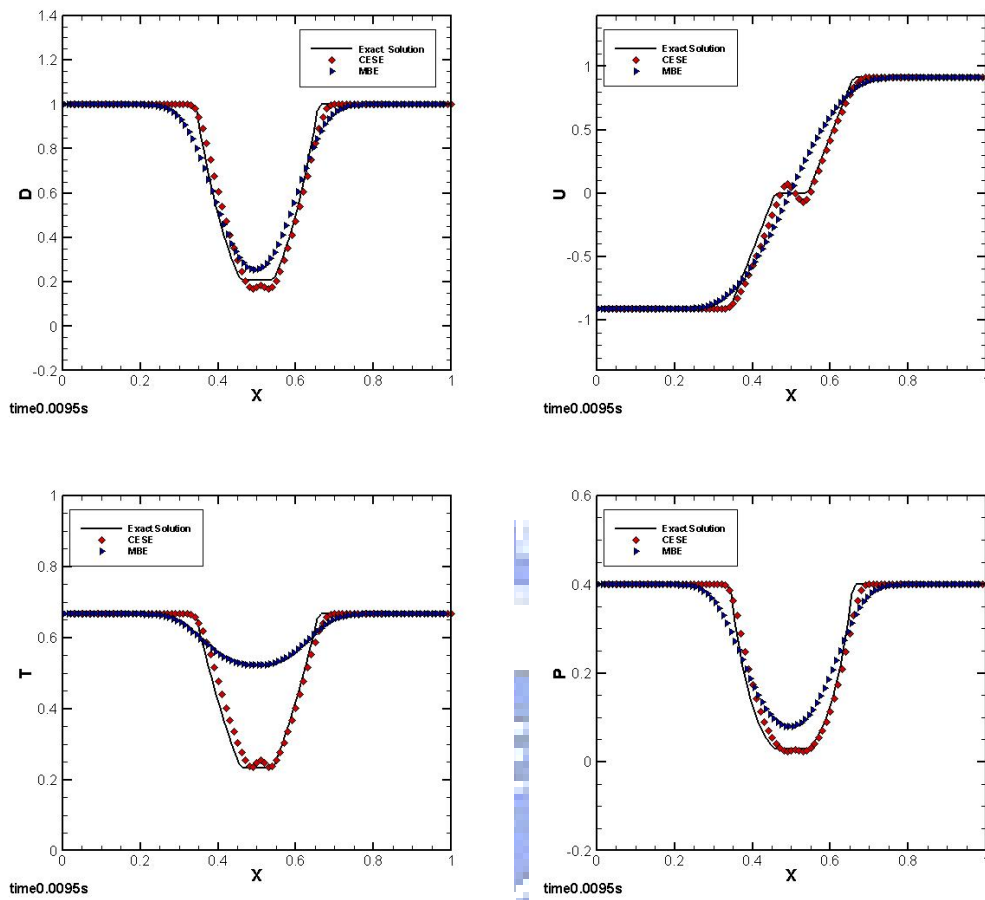
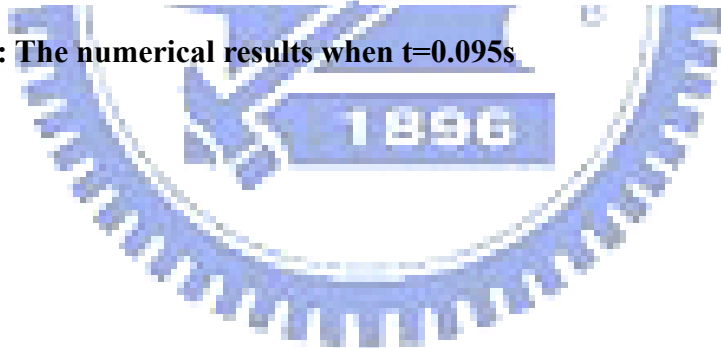


Fig.22 Test 4: The numerical results when $t=0.095s$



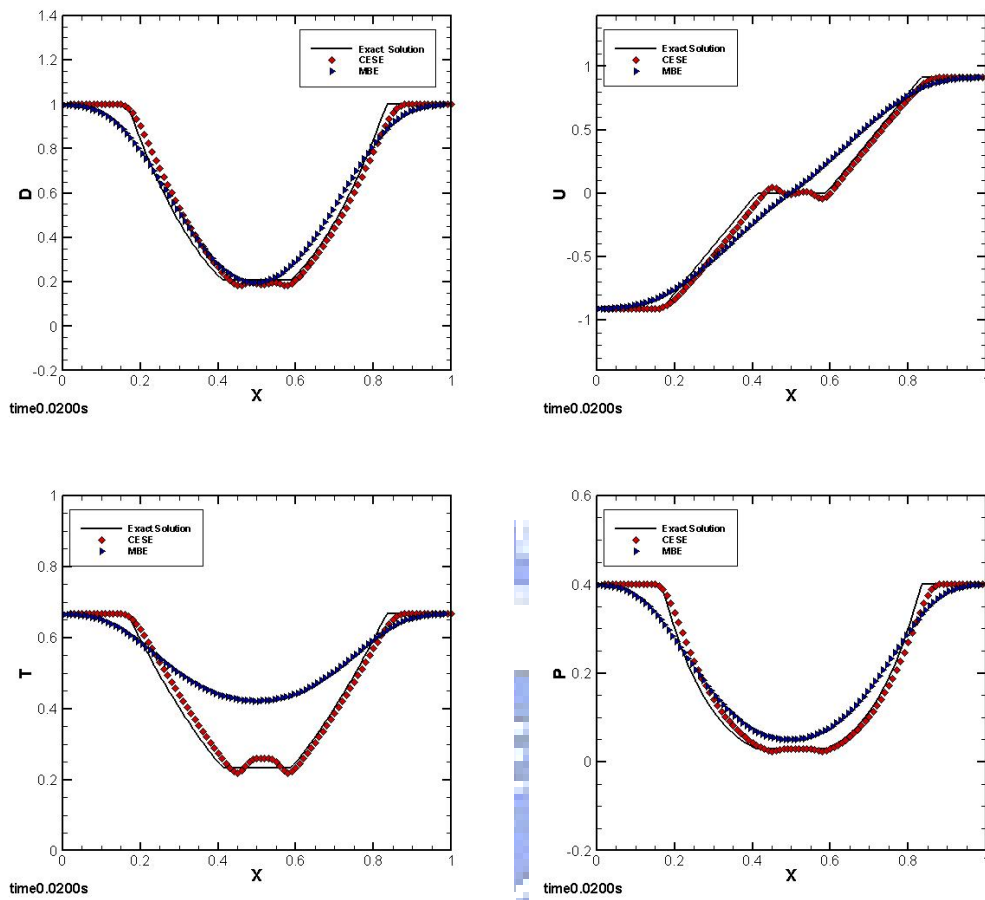
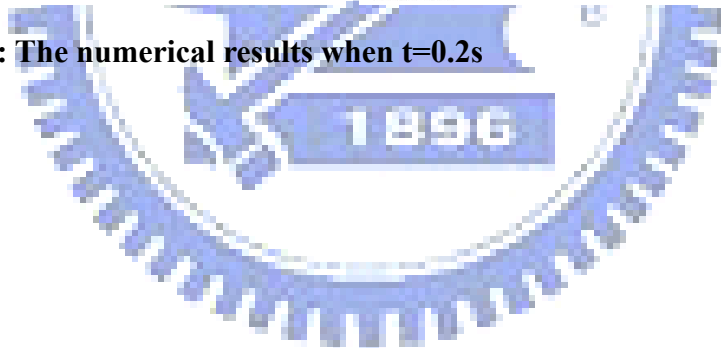


Fig.23 Test 4: The numerical results when $t=0.2s$



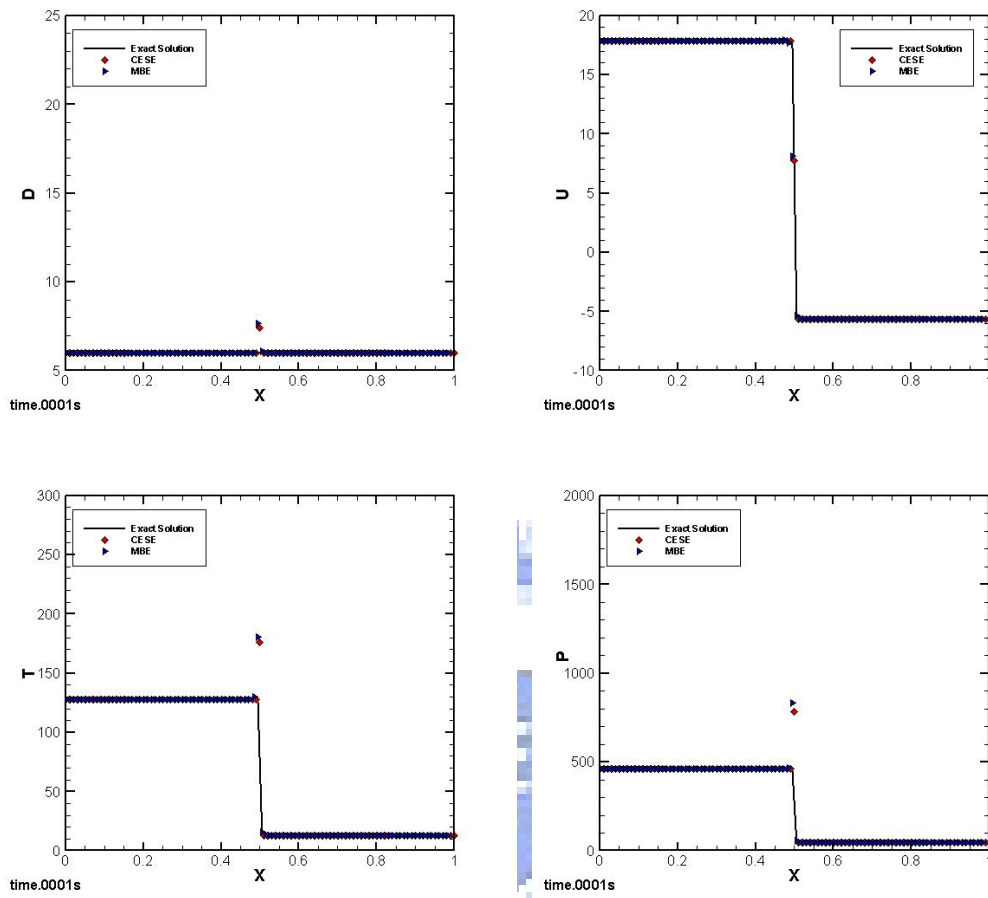


Fig.24 Test 5: The numerical results when $t=0.0001$ s



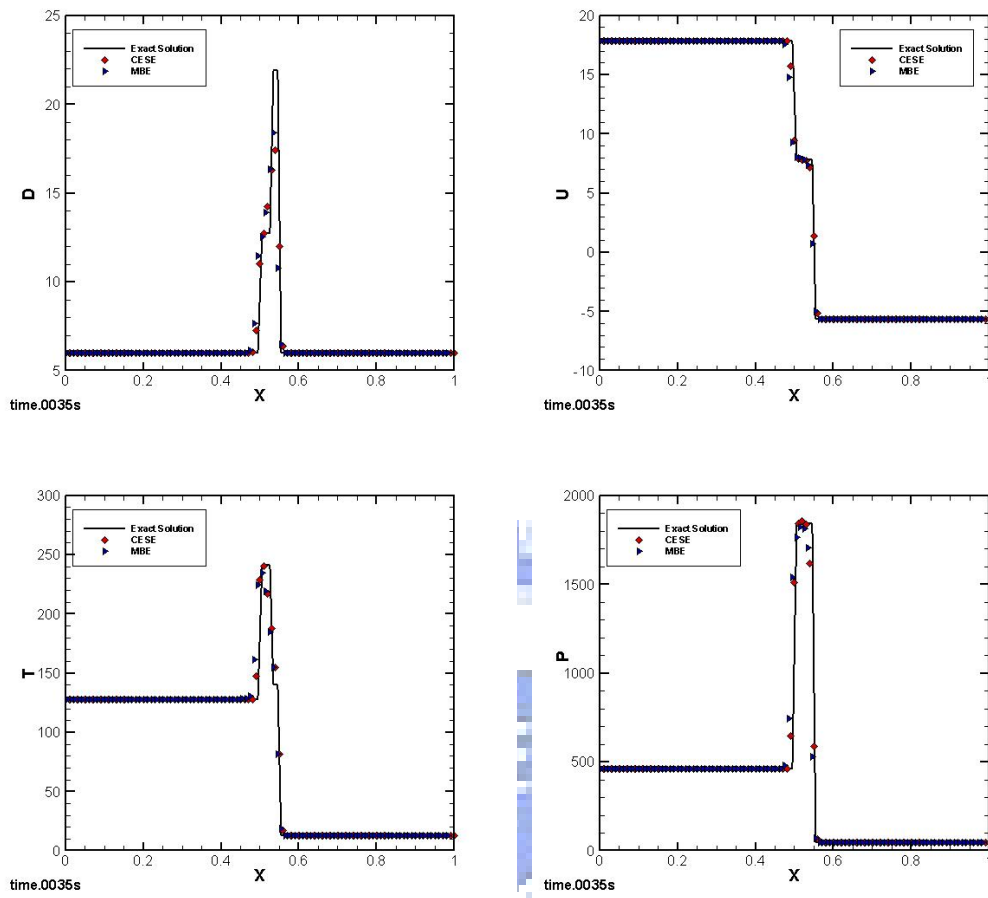


Fig.25 Test 5: The numerical results when $t=0.0035s$



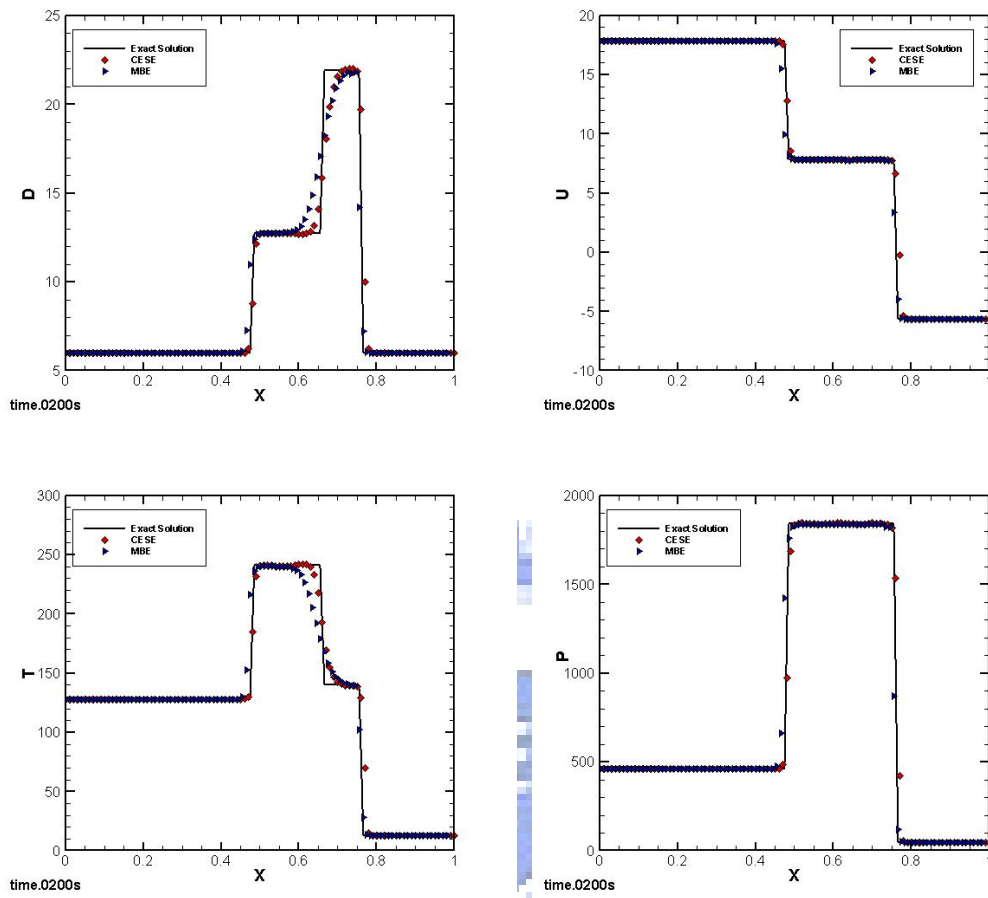


Fig.26 Test 5: The numerical results when $t=0.02s$



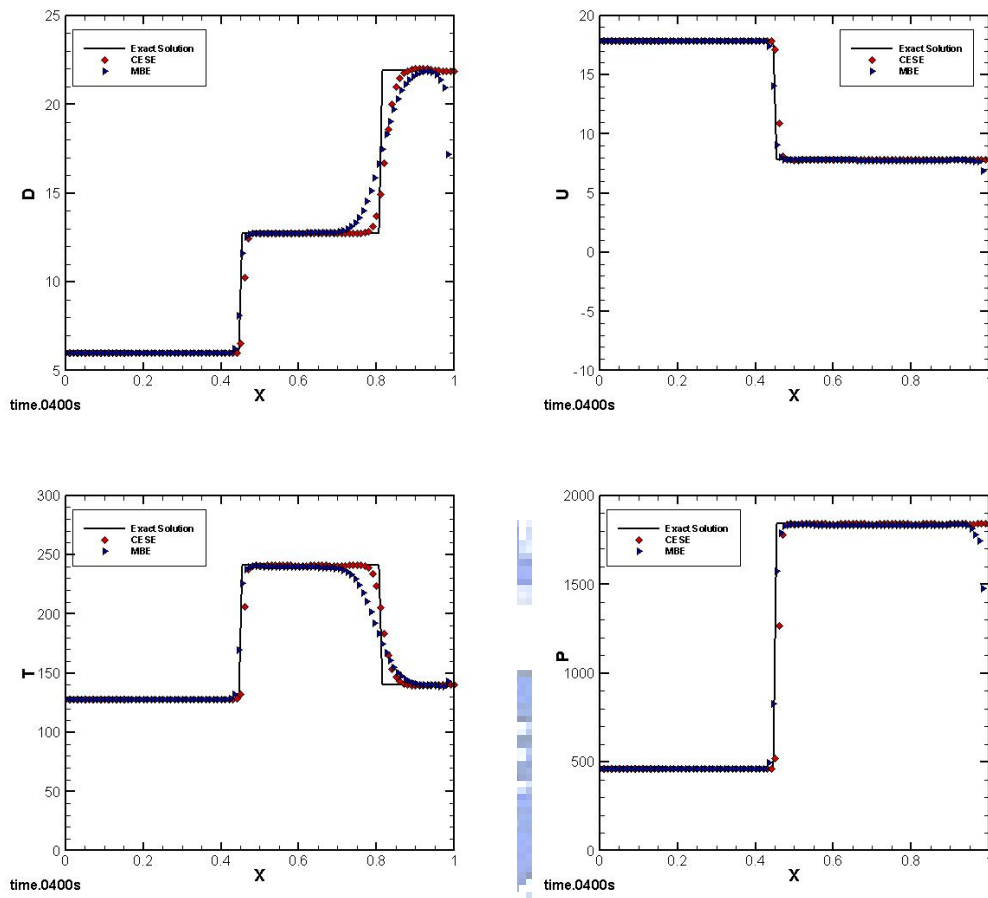


Fig.27 Test 5: The numerical results when $t=0.04s$



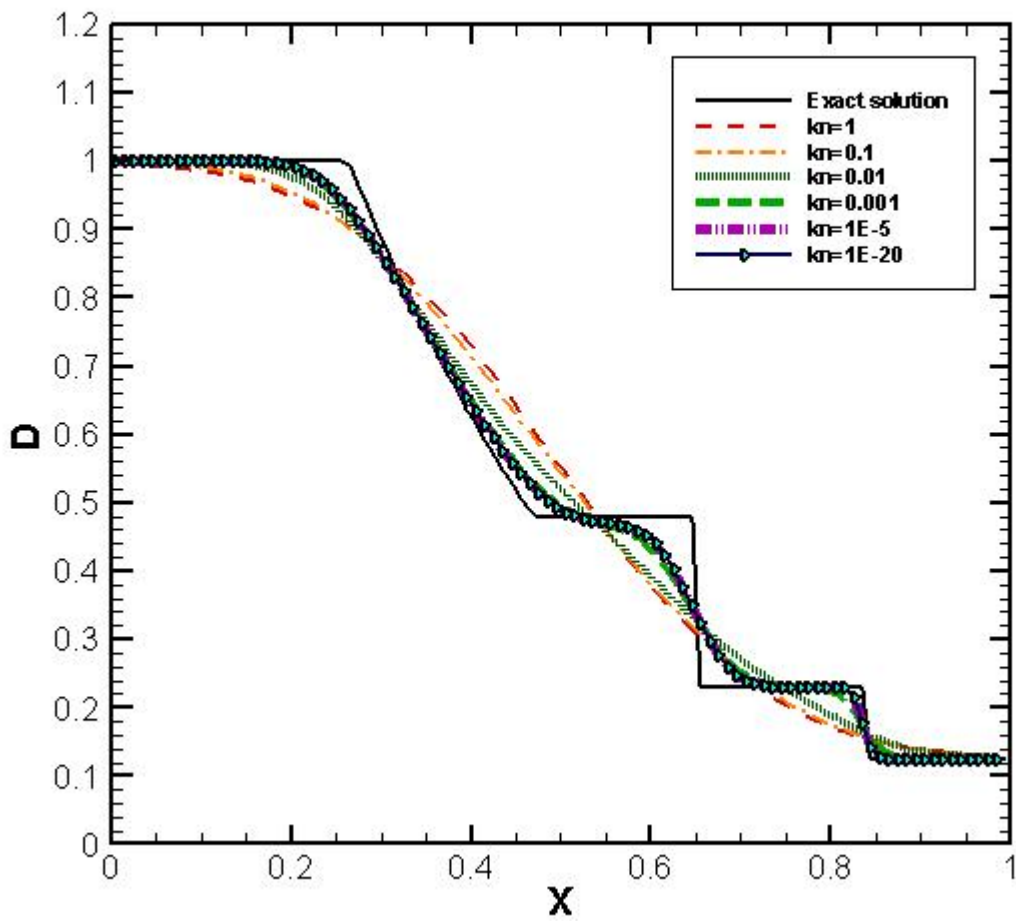


Fig.28 Test 1: Simulation of density in different Knudsen number of results when $t = 0.2s$



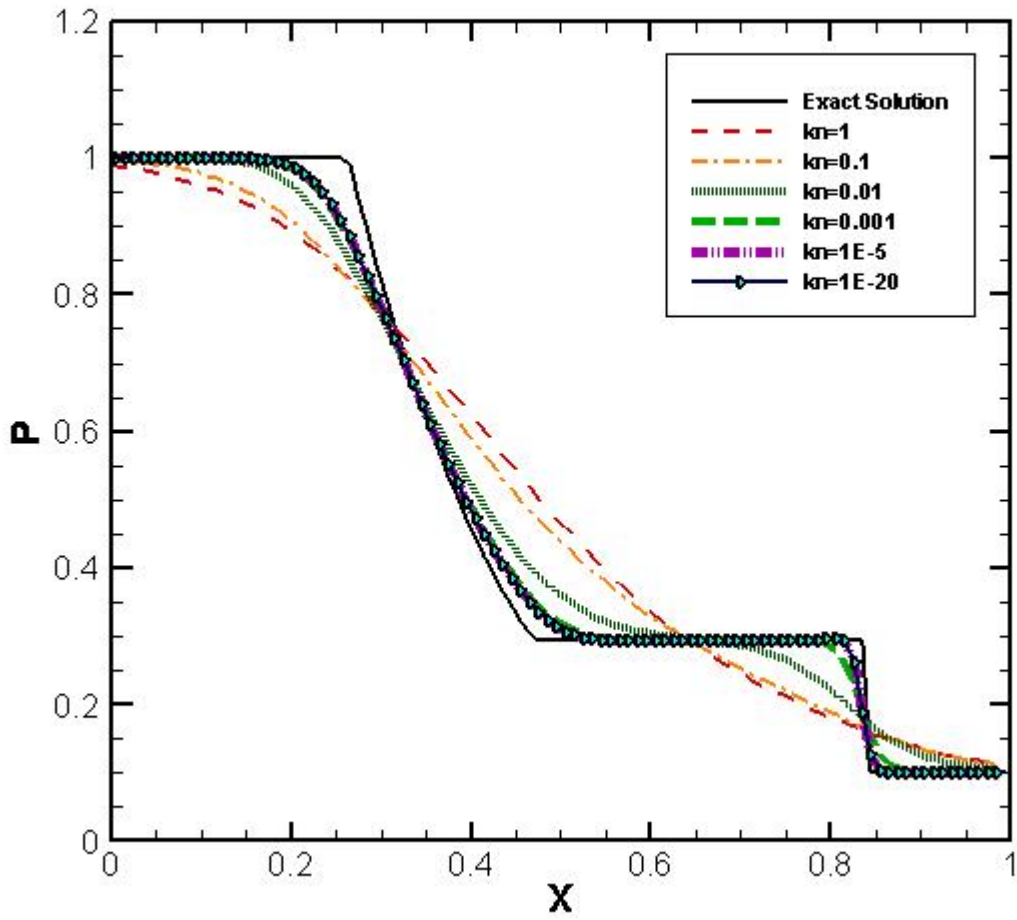
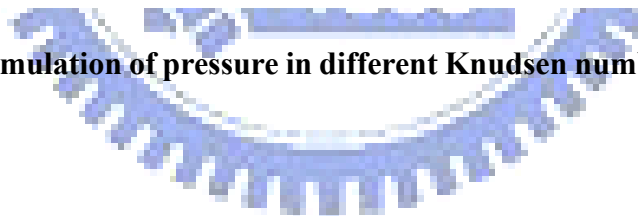


Fig.29 Test 1: Simulation of pressure in different Knudsen number of results when $t = 0.2s$



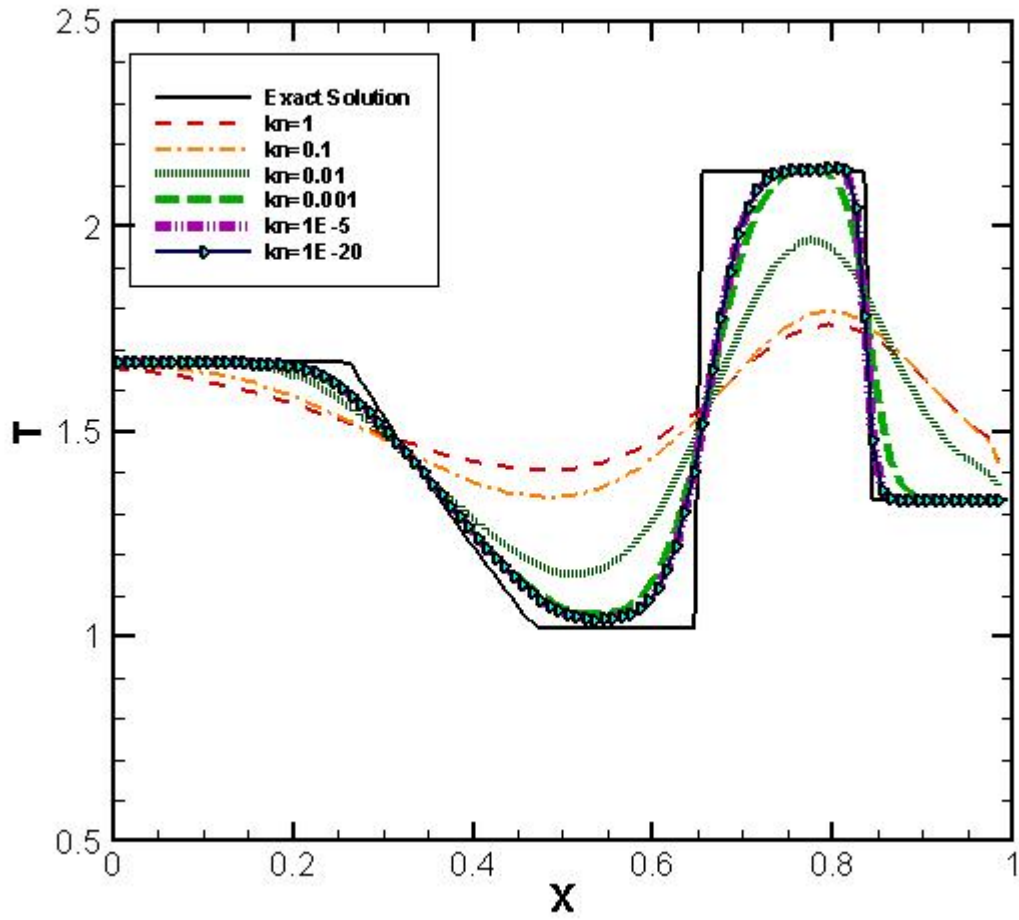
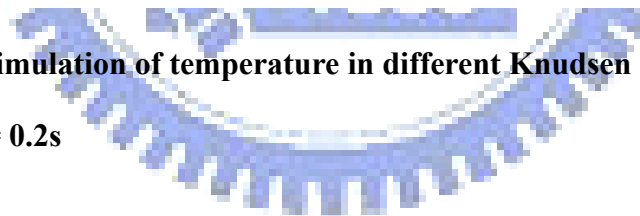


Fig.30 Test 1: Simulation of temperature in different Knudsen number of results when $t = 0.2s$



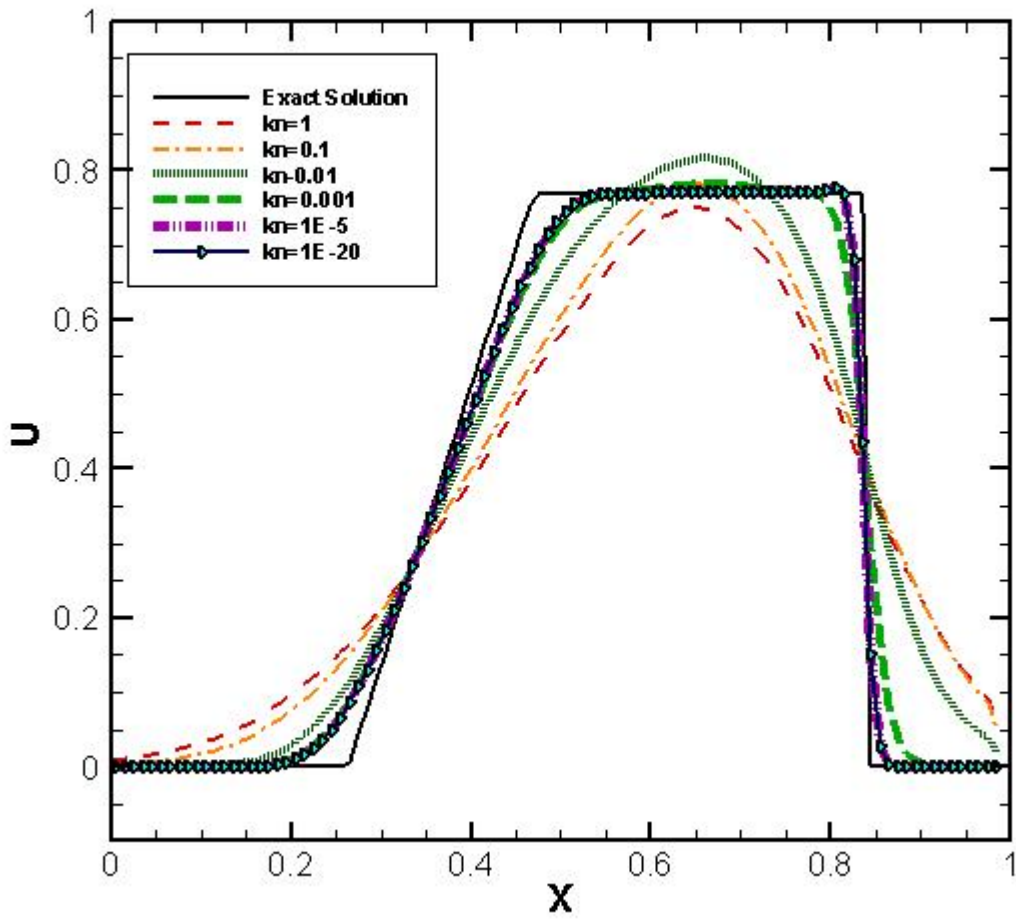


Fig.31 Test 1: Simulation of velocity in different Knudsen number of results when $t = 0.2s$

